Effects of Chain Length on the Mechanism and Rates of Metal-Catalyzed Hydrogenolysis of *n*-Alkanes

David D. Hibbitts,[†,§] David W. Flaherty,[†,‡] and Enrique Iglesia*,[†]

[†]Department of Chemical Engineering, University of California at Berkeley, Berkeley, California 94720, United States
[‡]Department of Chemical and Biomolecular Engineering, University of Illinois at Urbana−Champaign, Urbana, Illinois 61801, United States

S *Supporting Information*

ABSTRACT: C−C cleavage in C_2−C_{10} *n*-alkanes involves quasi-equilibrated C−H activation steps to form dehydrogenated intermediates on surfaces saturated with H atoms. These reactions are inhibited by H_2 to similar extents for C−C bonds of similar substitution in all acyclic and cyclic alkanes and, thus, show similar kinetic dependences on H_2 pressure. Yet, turnover rates depend sensitively on chain length because of differences in activation enthalpies ($\Delta H^{\ddagger}$) and entropies ($\Delta S^{\ddagger}$) whose mechanistic origins remain unclear. Density functional theory (DFT) estimates of $\Delta H^{\ddagger}$ and $\Delta G^{\ddagger}$ for C−C cleavage via >150 plausible elementary steps for propane and *n*-butane reactants on Ir show that hydrogenolysis occurs via α,β-bound RC*−C*R′[‡] transition states (R = H, C_xH_{2x+1}) in which two H atoms are removed from each C*. Calculated $\Delta H^{\ddagger}$

values decrease with increasing alkane chain length (C_2−C_8), consistent with experiment, because attractive van der Waals interactions with surfaces preferentially stabilize larger transition states. A concomitant increase in $\Delta S^{\ddagger}$, evident from experiments, is not captured by periodic DFT methods, which treat low-frequency vibrational modes inaccurately, but statistical mechanics treatments describe such effects well for RC*−C*R[‡] species, as previously reported. These findings, together with parallel studies of the cleavage of more substituted C−C bonds in branched and cyclic alkanes, account for the reasons that chain length and substitution influence $\Delta H^{\ddagger}$ and $\Delta S^{\ddagger}$ values and the dependence of rates on H_2 pressure and consequently explain differences in hydrogenolysis reactivities and selectivities across all alkanes.
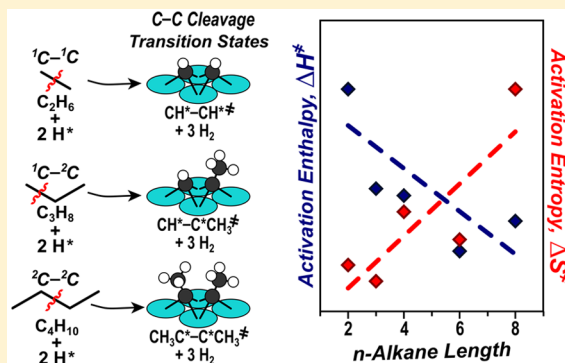
1. INTRODUCTION

The selective cleavage of specific C−C bonds on metals is a useful strategy to decrease the length of acyclic alkanes and to open rings in cycloalkanes,[1−6] but hydrogenolysis is an undesired side reaction in catalytic reforming and isomerization of refinery streams.[7−9] The cleavage of these C−C bonds occurs within extensively dehydrogenated hydrocarbons bound on metal surfaces[10−16] in a process that weakens C−C bonds by systematically replacing C−H bonds with C−M bonds (M = surface metal atom) and thereby increasing the occupancy of antibonding orbitals in C−C bonds.[17,18] These dehydrogenated transition states form H_2(g) and lead to large and positive activation entropies that compensate for the significant activation enthalpies of hydrogenolysis reactions. The formation of these dehydrogenated transition states is disfavored by thermodynamics at high H_2 pressures, leading to strong H_2 inhibition effects for hydrogenolysis of *n*-alkanes and branched acyclic and cyclic alkanes on Ir, Pt, Rh, and Ru catalysts.[11−13,19−27] C−C bond rupture turnover rates depend on the degree of substitution at the C atoms involved[19,26] and on the chain length of the products formed upon C−C cleavage, as shown by rates of ^2C−^2C cleavage in *n*-alkanes (^1C, ^2C, ^3C, and ^4C indicate primary, secondary, tertiary, and quaternary C

atoms, respectively), which vary with reactant chain length and with the location of the cleaved C−C bond along the *n*-alkane backbone.[28] The origins of these rate differences have been attributed to changes in reaction mechanisms or in the energies or structures of intermediates.[11−13,19−27] The structure and H content of the reactive intermediates involved, however, can only be inferred indirectly from the measured effects of H_2 pressure on C−C rupture rates in experimental studies[11−13,19−27] because such species exist in low concentrations during catalysis and are difficult to distinguish from inactive spectator adspecies by spectroscopic methods. As a result, their identities, and the reasons for large differences in C−C rupture rates, are accessible only through rigorous theoretical treatments.[22,29−33]

A general sequence of elementary steps for C−C hydrogenolysis is depicted in Scheme 1. These steps are consistent with measured rate data and lead to a rate equation that accurately predicts the effects of alkane and H_2 pressure on hydrogenolysis rates for ethane,[11−13,22−24,28,34] larger *n*-alkanes

Scheme 1. Proposed Mechanism for Alkane Hydrogenolysis on Metal Catalysts[a]

$$H_2 + 2* \overset{K_{H_2}}{\rightleftharpoons} 2\,H^* \tag{1.1}$$

$$C_nH_m + * \overset{K_{C_n}}{\rightleftharpoons} C_nH_m^* \tag{1.2}$$

$$C_nH_m^* + (l-1)* \overset{K_{CH,y}}{\rightleftharpoons} C_nH_{m-y}^{l*} + 0.5y\,H_2 \tag{1.3}$$

$$C_nH_{m-y}^{l*} \overset{k_{CC,y}}{\longrightarrow} C_aH_b^{c*} + C_{n-a}H_{m-y-b}^{d*} \tag{1.4}$$

$$C_aH_b^{c*} + x\,H^* \overset{0}{\rightleftharpoons} C_aH_{2a+2} + (c+x)* \tag{1.5}$$
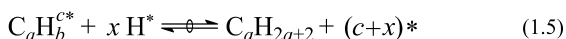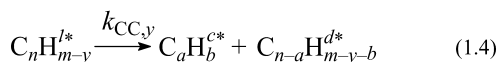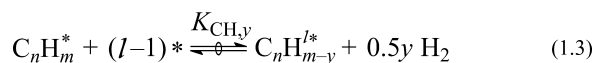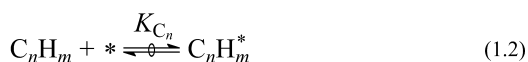
[a]The double half arror with a zero over it denotes a quasi-equilibrated reaction, * an unoccupied surface site, and $l*$ an adsorbate occupying l surface sites, and K_x and k_x are equilibrium and rate constants for individual steps.

(C_3–C_{10}),[25,28,35,36] branched alkanes (C_4–C_6)[19,25,37] and alkyl cyclohexanes.[19,38] Previous rate data for C–C cleavage within linear and branched alkanes and cycloalkanes showed that ^{1}C–^{1}C, ^{1}C–^{2}C, and ^{2}C–^{2}C bonds cleave at rates proportional to $\sim(H_2)^{-3}$ at high H_2:C_nH_m ratios (>100) on Ir, Rh, and Ru surfaces with chemisorbed hydrogen (H*) as the most abundant surface intermediate (MASI).[22,28] The inhibition by H_2 reflects quasi-equilibrated desorption of chemisorbed hydrogen (H*) (Step 1.1 in Scheme 1) and alkane adsorption and dehydrogenation events (Steps 1.2 and 1.3) to form transition states with the composition $C_nH_{(2n+2)-y}^{l*}$ bound at l sites on the catalyst surface, such that

$$\lambda = 1/2(y + l) = 3 \tag{1}$$

where λ is the exponent of the H_2 pressure term in the rate equation (3 for C–C cleavage within n-alkanes) and y is the number of H atoms removed via alkane dehydrogenation events (Step 1.3). The values of y and l cannot be determined independently from measured values of λ. Theoretical methods must therefore be used to determine the degree of dehydrogenation (y) of the predominant reactive intermediates, the

required number of catalytic binding sites (l), as well as their structure.

Density functional theory (DFT) calculations were previously used to probe ethane hydrogenolysis pathways on Ir(111) surfaces by examining C–H and C–C bond activations of all possible $C_2H_x^*$ intermediates (where $0 \leq x \leq 6$).[22] This work showed that (i) C_2H_6 is quasi-equilibrated with $C_2H_x^*$ intermediates ($2 \leq x \leq 6$) and (ii) C–C activation occurs via

$$CH_3CH_3 + 2H^* \overset{0}{\rightleftharpoons} CH^*CH^* + 3H_2 \tag{2}$$

$$CH^*CH^* \longrightarrow 2\,CH^* \tag{3}$$
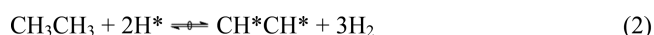
where the double half arrow with a zero over it in eq 2 indicates a quasi-equilibrated reaction. C–C bond cleavage in the preferred *CHCH* intermediate (eq 3) gives y and l values of 4 and 2, respectively, and thus a λ value of 3. This predicted λ value is consistent with measured λ values for ethane hydrogenolysis (20 kPa ethane, 0.4–2.0 MPa H2, 593 K) on 0.7 nm Ir (3.0 ± 0.2),[28] 7 nm Ir (3.3 ± 0.2),[22] and 0.9 nm Rh (3.0 ± 0.2)[28] clusters. The λ values for ethane are similar to those measured for larger (C_3–C_{10}) n-alkanes; such resemblance suggests that transition states with similar extents of dehydrogenation and surface coordination account for ^{2}C–^{1}C and ^{2}C–^{2}C bond cleavages in longer n-alkanes (C_3–C_{10})[28]

$$RCH_2CH_2R' + 2H^* \overset{0}{\rightleftharpoons} RC^*CR'^* + 3H_2 \tag{4}$$

$$RC^*C^*R'^* \longrightarrow RC^* + R'C^* \tag{5}$$

Neither experiment nor theory have yet to unequivocally demonstrated that two adjacent metal atoms are required to bind the vicinal C atoms in the C–C bond being cleaved (eq 4), each of which has lost two H atoms. Larger (C_3–C_{10}) n-alkanes may instead react via mechanisms and intermediates that differ significantly from the α,β-coordinated (Figure 1) structures involved in the cleavage of the C–C bond in ethane.[22] Longer n-alkane chains introduce backbone flexibility, thus allowing more diverse surface coordinations.[10,15,19,26,30−32] The rupture of C–C bonds in propane, for instance, could involve α,γ-bound metallacycle intermediates
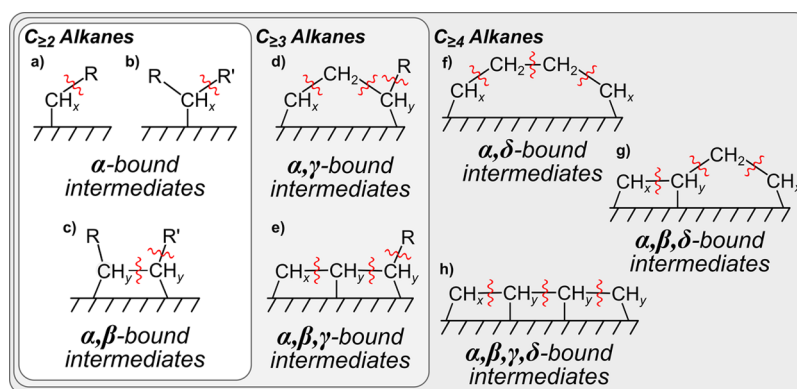
Figure 1. Types of partially dehydrogenated intermediates derived from $C_{\geq 2}$ alkanes showing C–C cleavage reactions of (a) α-bound intermediates via CH_x^*–$R^{\ddagger}$ (where $\ddagger$ indicates a transition state, $x = 0$–2 throughout figure), (b) α-bound intermediates via RCH_x^*–$R^{*\ddagger}$, (c) α,β-bound intermediates via RCH_y^*–$CH_y^*R'^{\ddagger}$ and $RCH_x^*CH_y^*$–$R^{*\ddagger}$ ($y = 0$–1 throughout figure), (d) α,γ-bound intermediates via CH_x^*–$CH_2^*CH_y^*R^{\ddagger}$, $CH_x^*CH_2^*$–$CH_y^*R^{\ddagger}$, and $CH_x^*CH_2^*CH_y^*$–$R^{\ddagger}$, (e) α,β,γ-bound intermediates via CH_x^*–$CH_y^*CH_y^*R^{\ddagger}$, $CH_x^*CH_y^*$–$CH_y^*R^{\ddagger}$, and $CH_x^*CH_y^*CH_y^*$–$R^{\ddagger}$, (f) α,δ-bound intermediates via CH_x^*–$*CH_2CH_2CH_x^{*\ddagger}$, $CH_x^*CH_2^*$–$CH_2CH_x^{*\ddagger}$, and $CH_x^*CH_2CH_2^*$–$CH_x^{*\ddagger}$, (g) α,β,δ-bound intermediates via CH_x^*–$CH_y^*CH_2CH_x^{*\ddagger}$, $CH_x^*CH_y^*$–$CH_2CH_x^{*\ddagger}$, and $CH_x^*CH_y^*CH_2$–$CH_x^{*\ddagger}$, and (h) $\alpha,\beta,\gamma,\delta$-bound intermediates via CH_x^*–$CH_y^*CH_y^*CH_x^{*\ddagger}$, $CH_x^*CH_y^*$–$CH_y^*CH_x^{*\ddagger}$, and $CH_x^*CH_y^*CH_y^*$–$CH_x^{*\ddagger}$.

$$CH_3CH_2CH_3 + 2H^* \rightleftharpoons {}^*CH_2CH_2CH^* + 2.5\,H_2 \qquad (6)$$

$${}^*CH_2CH_2CH^* + H^* \longrightarrow {}^*CH_2CH^* + CH^* + 0.5\,H_2 \qquad (7)$$

which cannot form from C_2H_6. Alternatively, propane and larger n-alkanes may cleave C−C bonds within α,β,γ-bound intermediates

$$CH_3CH_2CH_3 + 3H^* \rightleftharpoons {}^*CH_2CH^*CH_2^* + 3H_2 \qquad (8)$$

$${}^*CH_2CH^*CH_2^* \longrightarrow {}^*CH_2CH^* + CH_2^* \qquad (9)$$
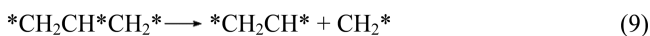
These reactions (eqs 4−9), and many other possibilities, could form 3 H_2(g) along with the C−C rupture transition state and thus be consistent with the H_2 inhibition observed for n-alkane hydrogenolysis.

Here, we examine the Ir-catalyzed (where Ir was chosen because of the prevalence of kinetic data[19,22,28,38] and prior DFT studies[22,26]) cleavage of ${}^1C-{}^2C$ and ${}^2C-{}^2C$ bonds using DFT methods. C−C cleavage steps are examined in α- and α,β-bound intermediates (similar to those possible during ethane hydrogenolysis), in α,γ- and α,δ-bound metallacyclic intermediates, and in intermediates with 3 or 4 C atoms bound at surfaces (α,β,γ-, α,β,δ-, α,γ,δ-, and $\alpha,\beta,\gamma,\delta$-bound intermediates). DFT-derived activation enthalpies and free energies indicate that cleavage of ${}^1C-{}^1C$, ${}^1C-{}^2C$, and ${}^2C-{}^2C$ bonds all occur via α,β-bound RC*−C*R'‡ transition states, irrespective of the chain length or the location of the C−C bond. Furthermore, we examine the effects of chain length and structure by calculating activation enthalpies and free energies for C−C cleavage in C_3-C_8 n-alkanes and cyclohexane.

2. METHODS

Periodic, plane-wave density functional theory (DFT) calculations were performed using the Vienna *ab initio* simulation package (VASP),[39−43] using procedures reported in detail elsewhere.[22,26] Planewaves were constructed using projector-augmented wave (PAW) potentials with an energy cutoff of 400 eV.[44,45] The revised Perdew−Burke−Ernzerhof (RPBE) form of the generalized gradient approximation (GGA) was used to describe exchange and correlation energies.[46−48] Additional calculations (discussed in Section 3.4) were performed using optB88-vdW,[49] optB86-vdW,[50] vdW-DF2,[51] and BEEF[52] functionals which all contain terms to capture van der Waals interactions. Transition state structures were obtained for each elementary reaction using nudged elastic band (NEB)[53,54] and dimer[55] methods. Further details of the computational methods are presented in previous works[22,26] and in the Supporting Information (SI, Section S1).

Here, apparent activation enthalpies ($\Delta H^{\ddagger}$) and free energies ($\Delta G^{\ddagger}$) are used to determine rates of C−C cleavage of intermediates derived from propane and butane, allowing theory to identify the structure of the active intermediate and transitions and how these may (or may not) depend on the size and carbon number of the reactant n-alkane. To do so, enthalpies and free energies of all reactant, transition, and product states are calculated at 593 K, the temperature at which λ was measured in previous work for ethane and n-alkanes.[19,22] Furthermore, $\Delta H^{\ddagger}$ and $\Delta G^{\ddagger}$ values are obtained for C−C cleavage via RC*−C*R'‡ transition states for C_3-C_6 n-alkanes and cyclohexane to examine the effects of chain length and structure (cyclic or acyclic). Calculations of reactants, products, and transition states for C−C cleavage of all intermediates were performed on Ir(111) surfaces without coadsorbed H* atoms.

H_2 desorption energies used in the determination of $\Delta H^{\ddagger}$ and $\Delta G^{\ddagger}$, in contrast, were calculated at 1 ML of H*.

The formalism of transition state theory[56] and the quasi-equilibrated nature of Steps 1.1−1.3 in Scheme 1 dictate that gaseous alkanes and l H* must be quasi-equilibrated with the C−C cleavage transition state ($C_nH_m^{l*\ddagger}$) and its λ H_2 products

$$C_nH_m + \ell H^* \underset{}{\overset{K^{\ddagger}}{\rightleftharpoons}} [C_nH_{m-y}^{\ell*}]^{\ddagger} + \lambda\,H_2 \qquad (10)$$
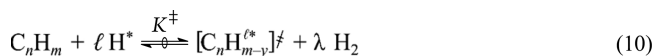
Here, $K^{\ddagger}$ is the equilibrium constant for the formation of the transition state from a gaseous alkane and a H*-covered surface. Consequently, $K^{\ddagger}$ (and thus rates of C−C activation) are related to the measured activation free energy ($\Delta G^{\ddagger}$) by

$$K^{\ddagger} = k_{CC,y} \frac{(\prod_{i=1}^{y} K_{CH,i})K_{C_n}}{(K_{H_2})^{\lambda}} = \frac{k_bT}{h}e^{(-\Delta G^{\ddagger}/RT)} \qquad (11)$$

$$\frac{r}{[L]} = \frac{k_bT}{h}e^{(-\Delta G^{\ddagger}/RT)}\frac{(C_nH_m)}{(H_2)^{\lambda}} \qquad (12)$$

Here, $\Delta G^{\ddagger}$ denotes the sum of the reaction free energies (ΔG_{rxn}) for all intervening steps involved in forming the reactive intermediate (from the gaseous alkane and the H*-covered surface) and the intrinsic free energy barrier (ΔG_{act}) for the elementary step that cleaves the C−C bond.

For example, the hydrogenolysis of ethane molecules involves C−C activation within CH*CH*, which involves the desorption of two H* atoms, the adsorption of C_2H_6, and the activation of C−H bonds to form the CH*CH* species that undergo C−C cleavage, prior to C−C rupture.[22] Consequently, the $\Delta G^{\ddagger}$ value for this reaction includes the adsorption free energy for H_2 ($\Delta G_{ads,H2}$, Step 1.1) and for C_2H_6 ($\Delta G_{ads,C2}$, Step 1.2), the free energies for the four C−H activation reactions that form CH*CH* from $C_2H_6^*$ ($\Sigma(\Delta G_{rxn,CH,i})$, Step 1.3), and the intrinsic free energy barrier for C−C activation of CH*CH* ($\Delta G_{act,CC,2}$, Step 1.4)

$$\Delta G^{\ddagger} = \Delta G_{act,CC,2} + \Sigma\Delta G_{rxn,CH,i} + \Delta G_{ads,C2} - 3\Delta G_{ads,H2} \qquad (13)$$

Substituting the free energies of formation for individual adsorbed and gas-phase species leads to

$$\Delta G^{\ddagger} = G[CH^*-CH^{*\ddagger}] + 3G[H_2(g)] - 2G[H^*] - G[C_2H_6(g)] \qquad (14)$$

which shows that the activation free energy only depends on the species directly shown in eq 10. Analogous equations exist for $\Delta H^{\ddagger}$ and $\Delta S^{\ddagger}$ values through their relation to $\Delta G^{\ddagger}$

$$\Delta G^{\ddagger} = \Delta H^{\ddagger} - T\Delta S^{\ddagger} \qquad (15)$$

The general form of eq 14

$$\Delta G^{\ddagger} = G[TS^{l*\ddagger}] + \lambda G[H_2(g)] - lG[H^*] - G[Alkane(g)] \qquad (16)$$

can be rewritten in terms of the free energy for dissociative H_2 adsorption (Step 1.1, $\Delta G_{ads,H2}$)

$$\Delta G^{\ddagger} = G[TS^{l*\ddagger}] + 0.5yG[H_2(g)] - 0.5l\Delta G_{ads,H2} - G[Alkane(g)] \qquad (17)$$

$\Delta G_{ads,H2}$ was calculated by desorbing 2 H* as H_2 from H*-saturated Ir(111) surfaces (1 H*/Ir$_{surf}$) to give enthalpies and
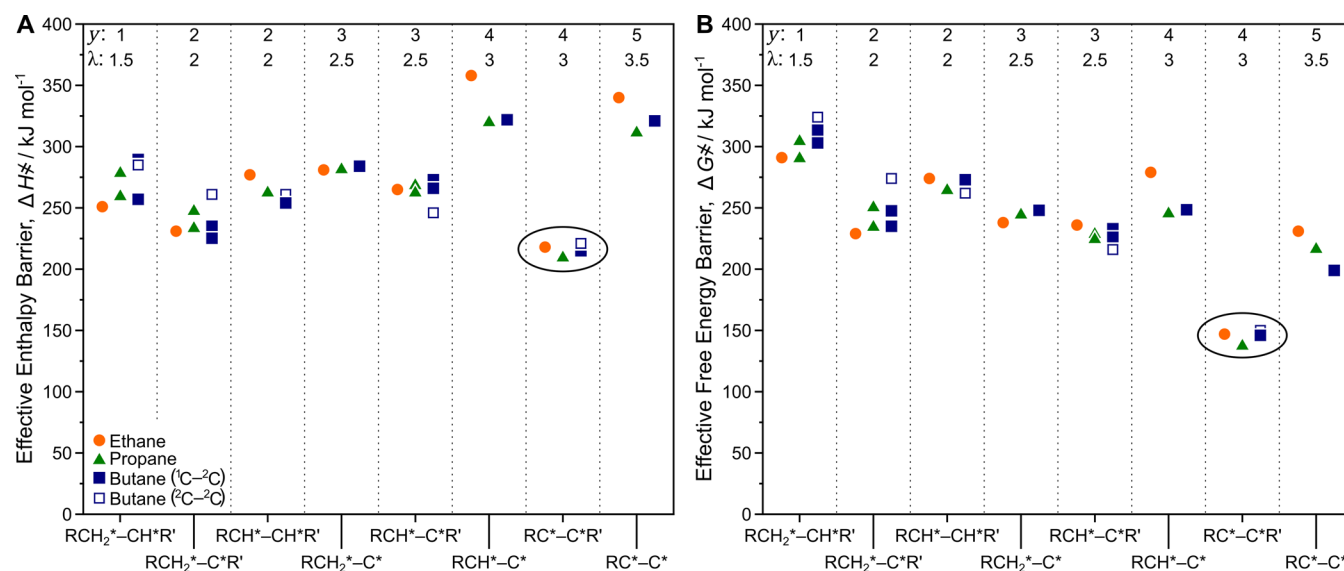
Figure 2. Calculated (A) $\Delta H^{\ddagger}$ and (B) $\Delta G^{\ddagger}$ values for C−C bond activation via α,β-bound transition states derived from ethane (●, orange), propane (▲, green), and butane ($^1C–^2C$, ■, $^2C–^2C$, □, blue). Within each bin of homologous transition states, points are organized according to alkane reactant. The number of H atoms removed from each transition state (relative to the alkane reactant (y)) and the total number of H_2 formed during the formation of each transition state from H*-covered surfaces (λ) are labeled along the top for reference. Table S1 in the SI shows y, l, λ, intrinsic enthalpy barriers (ΔH_{act}), $\Delta H^{\ddagger}$, $\Delta S^{\ddagger}$, and $\Delta G^{\ddagger}$ for each reaction.

free energies for dissociative H_2 ($\Delta H_{ads,H2} = -34$ kJ mol^{-1} and $\Delta G_{ads,H2} = -10$ kJ mol^{-1}) consistent with high H* coverages at >500 kPa H_2.[22] Here, enthalpies and free energies of all reactant, transition, and product states are calculated at 593 K, the temperature at which λ was measured in previous work for ethane and n-alkanes.[19,22]

3. RESULTS AND DISCUSSION

3.1. C−C Bond Cleavage of C_2−C_4 n-Alkanes in α- and α,β-Bound Intermediates. Ethane and larger n-alkanes can undergo dehydrogenation to form α-bound intermediates (e.g., CH_3CH^*) that can cleave C−C bonds via $CH_x^*-R^{*\ddagger}$ transition states. These C−C cleavage reactions can occur in species bound to surfaces through ^1C or ^2C atoms (in $C_{\geq 3}$ n-alkanes), as shown in Figure 1a and 1b, respectively. C−H activation at a vicinal C atom then forms α,β-bound intermediates (e.g., $CH_2^*CH_2^*$) that undergo C−C cleavage via $RCH_x^*-CH_x^*R'^{\ddagger}$ ($x = 0-1$) transition states (Figure 1c). The relative contributions of each of these transition states to hydrogenolysis rates depends on their respective $\Delta H^{\ddagger}$ and $\Delta G^{\ddagger}$ values, referenced to gaseous ethane, propane, or butane reactants.

$\Delta H^{\ddagger}$ and $\Delta G^{\ddagger}$ values for C−C cleavage in α-bound and α,β-bound intermediates derived from ethane, propane, and butane are shown in Figure 2 (Table S1 shows individual intrinsic enthalpy barriers (ΔH_{act}) and $\Delta S^{\ddagger}$). C−C cleavage via α,β-bound $RC^*-C^*R'^{\ddagger}$ ($y = 4$, $l = 2$) structures have the lowest $\Delta H^{\ddagger}$ (Figure 2A) and $\Delta G^{\ddagger}$ (Figure 2B) values for each of the three n-alkanes among all C−C cleavage reactions of α- and α,β-bound species. The $\Delta G^{\ddagger}$ values for C−C cleavage via $RC^*-C^*R'^{\ddagger}$ are ~50 kJ mol^{-1} lower than those for all other $RCH_x^*-CH_x^*R'^{\ddagger}$ ($x = 0-2$) transition states (Figure 2B), indicating that the other routes are unlikely to contribute to measured rates. For example, $C_{\geq 3}$ alkanes can also cleave their $RCH_x^*CH_x^*-R'^{\ddagger}$ ($x = 0-1$) bonds, in four distinct pathways. $\Delta H^{\ddagger}$ and $\Delta G^{\ddagger}$ values (shown in Table S2 of the Supporting Information, SI) for these reactions show that they do not

contribute to observed hydrogenolysis rates. C−C cleavage events in the $RC^*-C^*R'^{\ddagger}$ transition states, which have the lowest $\Delta G^{\ddagger}$ values and highest rates (at 593 K) among activations of α- and α,β-bound species, give λ values of 3 ($y = 4$, $l = 2$), consistent with those measured for the cleavage of all C−C bonds in these alkanes.[19,22,28] C−C cleavage reactions of select transition states bound with different coordination at metal surfaces (Figure 1d−h) may also give λ values of 3. These alternate routes cannot be distinguished from those mediated by $RC^*-C^*R'^{\ddagger}$ transition states by experiment, thus requiring theoretical treatments for comparisons. Next, we consider the activation of α,γ-bound and α,β,γ-bound intermediates (Figure 1d,e), which can be formed from $C_{\geq 3+}$ n-alkanes.

3.2.1. C−C Bond Cleavage of Propane and Butane in α,γ-Bound Metallacyclic Intermediates. Propane and butane reactants can cleave their C−C bonds via α,γ-bound metallacycles (e.g., $CH^*CH_2CH^*$) (Figure 1d). We consider here each of the 21 possible activations occurring via α,γ-bound metallacycles derived from propane and butane (details shown in Table S2, SI). These α,γ-bound intermediates can form alkenes directly upon C−C cleavage (without hydrogenation−dehydrogenation events)

$$CH_2^*CH_2CH^* + * \rightarrow CH_2^*CH_2^* + CH^* \quad (l = 3)$$
(18)
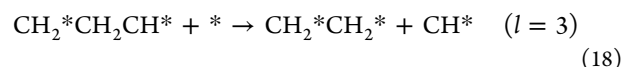
Here, we examine steps that retain the surface-bound alkene products (eq 18) and steps that desorb them directly (eq 19)

$$CH_2^*CH_2CH^* \rightarrow CH_2CH_2(g) + CH^* + * \quad (l = 2)$$
(19)
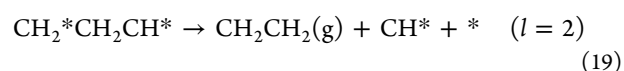
to assess their relative rates and whether two or three binding sites lead to more stable transition states. Intrinsic activation energy (ΔH_{act}) and C−C cleavage transition state structures were identical for both steps on bare Ir(111) surfaces; thus, we conclude that eq 18 will prevail on H*-covered surfaces by avoiding the free energy penalty required to desorb one additional H* atom. Thus, the transition states involved in C−C cleavage within these α,γ-bound intermediates bind onto two
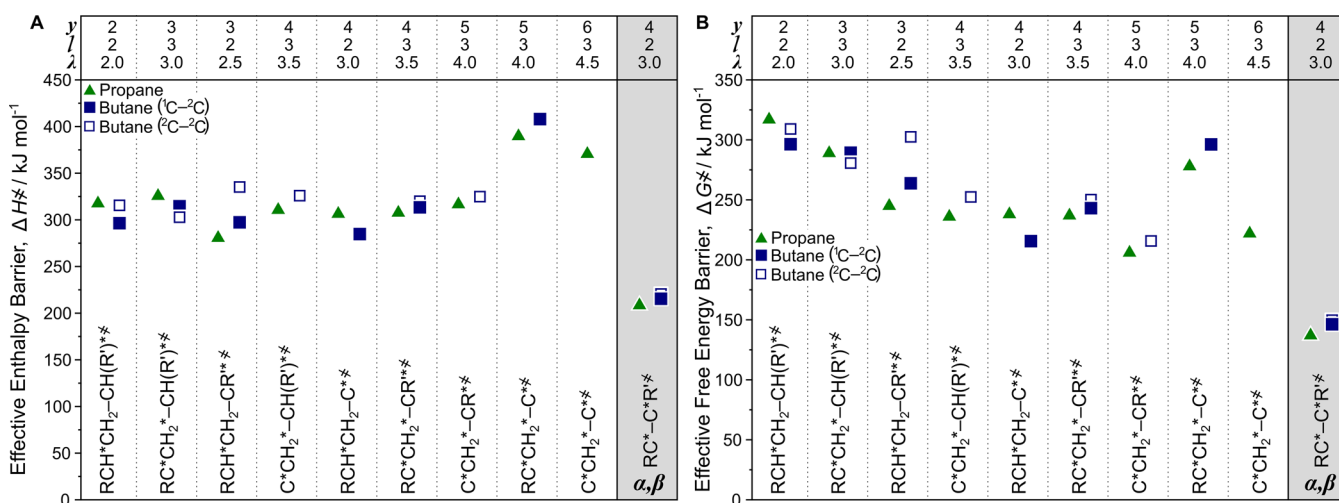
Figure 3. Calculated (A) $\Delta H^{\ddagger}$ and (B) $\Delta G^{\ddagger}$ values for C−C bond activation via α,γ-bound transition states in propane (▲, green) and butane (^{1}C−^{2}C, ■, ^{2}C−^{2}C, □, blue) (with cleavage via the most favorable α,β-bound RC*−C*R'‡ shown along the far right of each plot for reference). Within each bin of homologous transition states, points are organized according to alkane reactant. The number of H atoms removed from the alkane reagent to form each transition state (y), the number of sites required (l), and the total number of H_2 formed during the formation of each transition state from H*-covered surfaces (λ) are labeled along the top for reference. Table S3 in the SI shows y, l, λ, intrinsic enthalpy barriers (ΔH_{act}), $\Delta H^{\ddagger}$, $\Delta S^{\ddagger}$, and $\Delta G^{\ddagger}$ for each reaction.

or three sites, depending on whether an alkene is formed directly from the C−C cleavage transition state. These α,γ-bound intermediates react with $\Delta H^{\ddagger}$ values (282−372 kJ mol^{-1}) that are much larger than in α,β-bound intermediates for ethane, propane, and butane (CH*−CH*‡ species (218 kJ mol^{-1}), CH$_3$C*−CH*‡ species (207 kJ mol^{-1}), C$_2$H$_6$C*−CH*‡ (210 kJ mol^{-1}), or CH$_3$C*−C*CH$_3$‡ (215 kJ mol^{-1})) (Figure 3). These larger $\Delta H^{\ddagger}$ values for α,γ-bound intermediates may reflect the weak interactions between the ^{2}C atom and the metal surface, as shown by ^{2}C−M distances (237−350 pm) that are much longer than for α,β-bound RC*−C*R'‡ species (<210 pm), which appear to be stabilized by greater backdonation into antibonding C−C orbitals, thus weakening C−C bonds and giving rise to smaller $\Delta H^{\ddagger}$ values.[22]

The α,γ-bound intermediates contain two to six fewer H atoms than propane or butane; taken together with the required desorption of two H* atoms from Ir surfaces, these intermediates give λ values of 2.0−4.5 (Figure 3). These processes, which show a large range of λ values, lead to $\Delta S^{\ddagger}$ values between 1 and 251 J mol^{-1} K^{-1}, largely reflecting the number of H_2(g) evolved

$$\Delta S^{\ddagger} = S[CH_x*CH_2*-CH_y*R^{\ddagger}] + \lambda S[H_2(g)] - lS[H*] - S[C_3H_7R(g)] \tag{20}$$

$\Delta G^{\ddagger}$ values for C−C rupture in these α,γ-bound metallacycles range from 207 to 318 kJ mol^{-1}, and among these structures, activation via RC*−CH$_2$*C*‡ gives the smallest $\Delta G^{\ddagger}$ for C−C cleavage in propane-derived species (207 kJ mol^{-1}) and for ^{2}C−^{2}C activation in C$_4$ species (216 kJ mol^{-1}). The RC*−CH$_2$*C*‡ transition state, however, gives a λ value of 4, in contrast with the value of 3.0 measured for propane and butane.[28] Also, $\Delta H^{\ddagger}$ and $\Delta G^{\ddagger}$ values for C−C rupture in these metallacycles are much larger than for C−C cleavage via α,β-bound RC*−C*R'‡ transition states (Figure 3). These comparisons show that α,γ-bound metallacycles do not contribute detectably to n-alkane hydrogenolysis rates.

3.2.2. C−C Bond Cleavage via α,β,γ-Bound Intermediates in Propane and Butane. The activation of ^{3}C−^{x}C bonds in branched alkanes are more strongly inhibited by H_2 than for ^{1}C−^{2}C or ^{2}C−^{2}C bonds in the same alkanes, even though ^{3}C−^{x}C bonds have fewer H atoms that can be removed before C−C cleavage.[19,26] As a result, C atoms not involved in the C−C bond being cleaved must lose H atoms before C−C cleavage via intermediates that lose H atoms from three or more C atoms.[19,26,57] Such activations in propane and butane can form α,β,γ-bound intermediates (such as CH$_2$*C*CH*), which cannot be formed from ethane (Figure 1e). These intermediates may give lower C−C cleavage $\Delta G^{\ddagger}$ barriers than those with greater H content because of the entropy gains associated with the evolution of more H_2 molecules. In total, 42 α,β,γ-bound transition states can form from propane and butane reactants. For example, CH$_2$*C*CH* can cleave at one of two C−C bonds

$$CH_2*C*CH* \rightarrow CH*C* + CH_2* \tag{21}$$

$$CH_2*C*CH* \rightarrow CH_2*C* + CH* \tag{22}$$
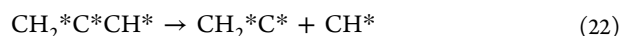
with $\Delta H^{\ddagger}$ values of 396 kJ mol^{-1} (eq 21) and 303 kJ mol^{-1} (eq 22) and $\Delta G^{\ddagger}$ values of 278 kJ mol^{-1} (eq 21) and 193 kJ mol^{-1} (eq 22). The transition state depicted in eq 22 has the smallest $\Delta H^{\ddagger}$ (303 kJ mol^{-1}) and $\Delta G^{\ddagger}$ (193 kJ mol^{-1}) values among all C−C bond activations in α,β,γ-bound intermediates derived from propane (Table S4 in SI shows data for all 18 C−C bond activations). Among the C−C cleavage pathways for butane-derived intermediates, these steps

$$CH_3CH*C*CH* \rightarrow CH_3CH*C* + CH* \tag{23}$$

$$CH_2*C*C*CH_3 \rightarrow CH_2*C* + CH_3C* \tag{24}$$
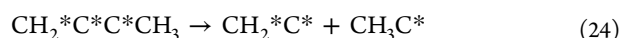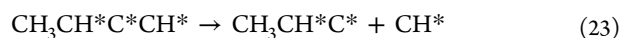
give the lowest $\Delta H^{\ddagger}$ and $\Delta G^{\ddagger}$ values for ^{1}C−^{2}C (295 and 182 kJ mol^{-1}) and ^{2}C−^{2}C cleavage (294 and 178 kJ mol^{-1}) of α,β,γ-bound intermediates derived from butane (Table S4 in SI shows data for all 24 C−C bond activations). These C−C cleavage transition states (eqs 23 and 24) are homologous (can be formed by the substitution of H atoms with alkyl groups) to
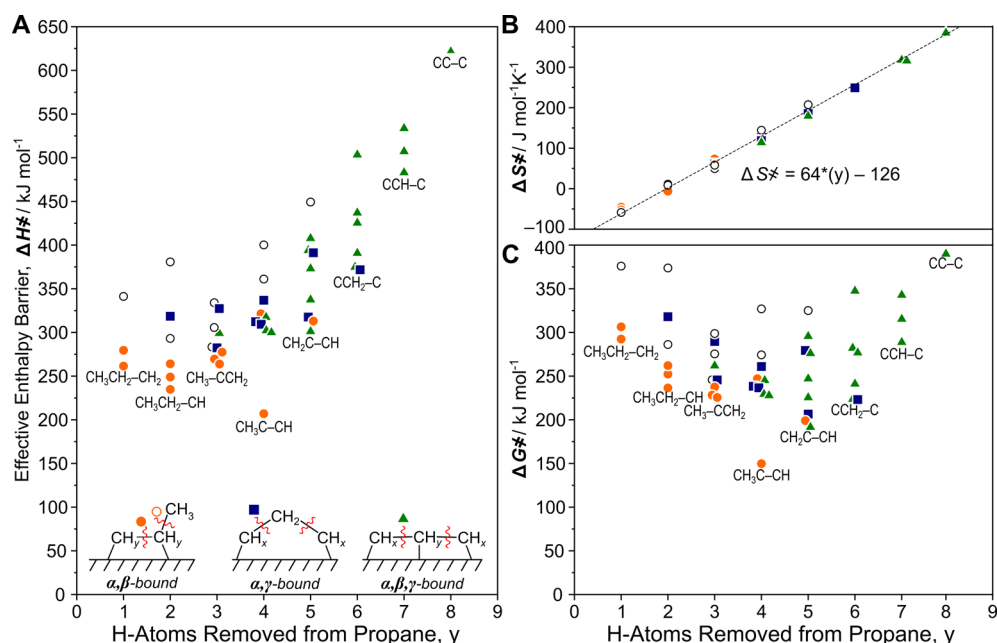
Figure 4. (a) $\Delta H^{\ddagger}$, (b) $\Delta S^{\ddagger}$, and (c) $\Delta G^{\ddagger}$ for C–C cleavage of propane-derived intermediates through: α,β-bound intermediates via $CH_3CH_x^*$–$CH_y^{*\ddagger}$ ($x = 0$–2, $y = 0$–3) (●, orange) and CH_3^*–$CH_xCH_y^{*\ddagger}$ (O, orange) transition states; α,γ-bound intermediates ($CH_x^*CH_2CH_y^*$, $x = 0$–2, $y = 0$–2, ■, blue); and α,β,γ-bound intermediates ($CH_x^*CH_y^*CH_z^*$, $x = 0$–2, $y = 0$–1, $z = 0$–2, ▲, green). The structure of the transition state with the lowest $\Delta H^{\ddagger}$ and $\Delta G^{\ddagger}$ is listed near the abscissa for each group with the same number of H atoms removed from propane. Tables S1–S4 in the SI show y, l, λ, intrinsic enthalpy barriers (ΔH_{act}), $\Delta H^{\ddagger}$, $\Delta S^{\ddagger}$, and $\Delta G^{\ddagger}$ for each reaction.

eq 22, indicating that the preferred activation of α,β,γ-bound C_3 or C_4 species is unaffected by chain length. C–C cleavage transition states for α,β,γ-bound C_3 or C_4 species, however, all show $\Delta H^{\ddagger}$ and $\Delta G^{\ddagger}$ barriers much higher than for propane or butane hydrogenolysis via α,β-bound RC^*–$C^*R'^{\ddagger}$ transition states, indicating that transition states stabilized by coordinating three contiguous C atoms to surfaces do not contribute to C–C rupture rates in propane or butane.

3.2.3. C–C Bond Cleavage in Propane. Figure 4 summarizes $\Delta H^{\ddagger}$ and $\Delta G^{\ddagger}$ values for all 48 different C–C rupture pathways in propane and shows that the lowest $\Delta H^{\ddagger}$ and $\Delta G^{\ddagger}$ barriers for C–C activation involve α,β-bound species for any given transition state composition. More specifically, C–C cleavage via CH_3C^*–$CH^{*\ddagger}$ gives the lowest $\Delta H^{\ddagger}$ (207 kJ mol^{-1}) and $\Delta G^{\ddagger}$ (150 kJ mol^{-1}) values among all routes, indicating that they predominantly account for measured rates. More unsaturated transition states give larger and more positive $\Delta S^{\ddagger}$ values than more saturated counterparts because of the larger number of evolved $H_2(g)$ molecules (eq 19), as evident from the effects of the number of H atoms removed from propane (y) on $\Delta S^{\ddagger}$ (Figure 4b). Transition state entropies differ by less than 43 J mol^{-1} K^{-1} among transition states with the same H-content (Tables S1–S4 in SI). As a result, differences among $\Delta G^{\ddagger}$ values for each set of isomers depend predominantly on their $\Delta H^{\ddagger}$ values, which accurately describe the relative contributions of the various isomeric transition states. $\Delta S^{\ddagger}$ values increase between isomeric transition states with different y values according to

$$\Delta S^{\ddagger} \ (\text{J mol}^{-1} \ \text{K}^{-1}) = 64*(y) - 126 \quad (25)$$

as shown in Figure 4b. The slope of this line (64 J mol^{-1} K^{-1} H^{-1}) is nearly equal to half the entropy of $H_2(g)$ (75 J mol^{-1} K^{-1}), which indicates that H atoms in transition states have just 15% of their gas-phase entropy. DFT-derived values for both $\Delta H^{\ddagger}$ and $\Delta G^{\ddagger}$ indicate that propane undergoes hydrogenolysis

via CH_3C^*–$CH^{*\ddagger}$, a transition state that is homologous of the CH^*–$CH^{*\ddagger}$ transition state that mediates ethane hydrogenolysis. DFT-derived λ values (3) agree with measured values (3.2 ± 0.3).[19,28] Yet, DFT-derived $\Delta H^{\ddagger}$ (207 kJ mol^{-1}) and $\Delta G^{\ddagger}$ (150 kJ mol^{-1}) differ slightly from experimental values (230 ± 3 kJ mol^{-1} and 133 ± 6 kJ mol^{-1} for $\Delta H^{\ddagger}$ and $\Delta G^{\ddagger}$, respectively); these deviations are discussed in detail in Section 3.4.

3.3.1. C–C Bond Cleavage in Butane via α,δ-Bound Intermediates. Butane-derived α,γ-bound metallacycles are unlikely to contribute significantly to hydrogenolysis rates because of their large $\Delta G^{\ddagger}$ values (section 3.2.1); yet, related α,δ-bound metallacycles (Figure 1f) have been implicated in C–C rupture reactions catalyzed by metal surfaces[9,12,57−62] and Ni- and Pt-centered organometallic complexes.[63−66] α,δ-Bound transition states have also been shown to mediate ^3C–^3C cleavage within 2,3-dimethylbutane on Ir(111)[26] via

$$C^*CH(CH_3)CH(CH_3)C^* \rightarrow 2CH_3CH^*C^* \quad (26)$$
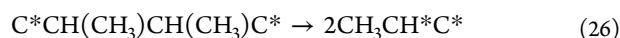
The $C^*CH(CH_3)$–$CH(CH_3)C^{*\ddagger}$ transition state structure involved in this reaction has ^3C–M distances (308 pm) that are inconsistent with the direct involvement of the metal surface in the cleavage of the ^3C–^3C bond, in stark contrast with the cleavage of C–C bonds in ethane (or propane/butane) via α,β-bound RC^*–$C^*R'^{\ddagger}$ transition states (C–M bond lengths <220 pm). n-Butane can also form α,δ-bound intermediates (Figure 1f), such as $CH_2^*CH_2CH_2CH_2^*$, which can form one or two C_2H_4 species upon cleavage of its ^2C–^2C bond via a process in which neither ^2C atom is dehydrogenated or bound to the surface at the reactant state, the transition state, or the product state

$$CH_2^*CH_2CH_2CH_2^* \rightarrow 2CH_2CH_2(g) + 2* \quad (27)$$

Alternatively, if a terminal C atom has formed more attachments to the surface than in eq 27 ($CH_2^*CH_2CH_2CH_x^*$,
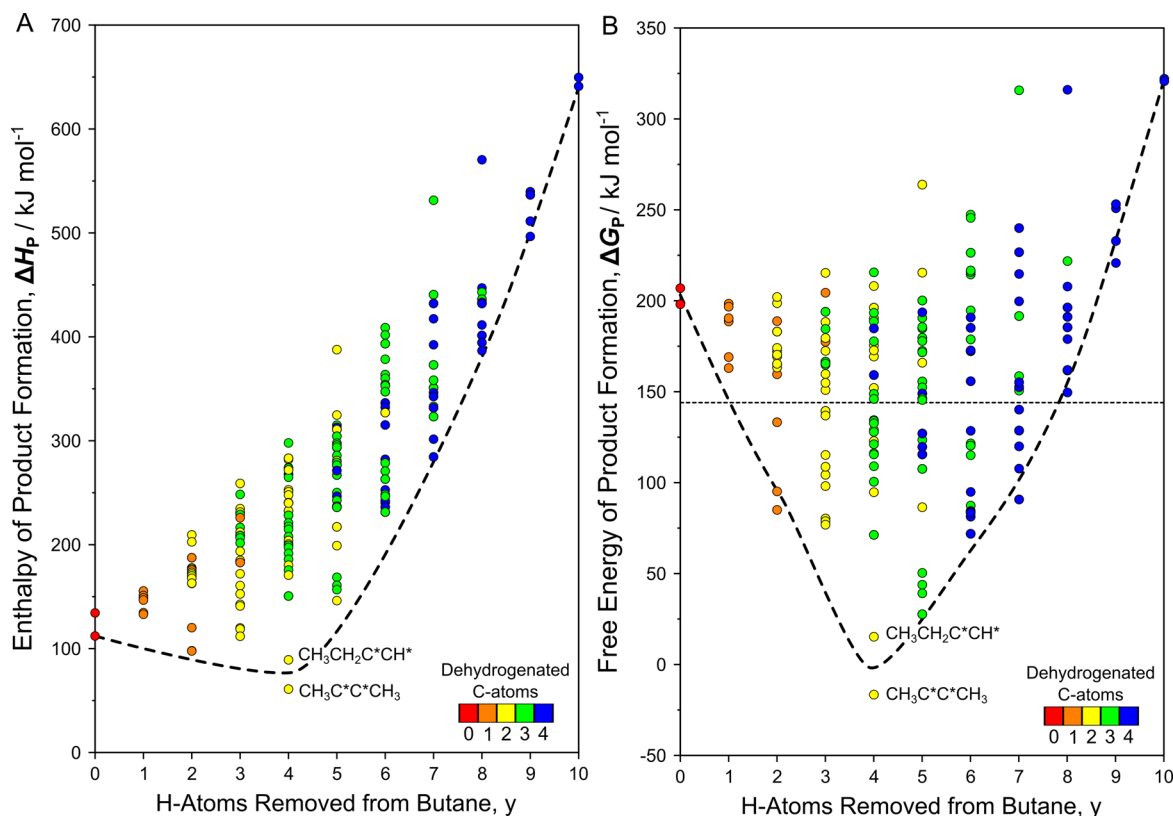
Figure 5. (A) Enthalpy and (B) free energy to form products (ΔH_P and ΔG_P) of all possible (223) C−C cleavage reactions of C_4 intermediates derived from *n*-butane. These ΔH_P and ΔG_P values represent lower bounds for $\Delta H^{\ddagger}$ and $\Delta G^{\ddagger}$ for butane activation. The color of the symbol represents the number of dehydrogenated C atoms (and thus attachments to the surface).

$x = 0-1$), a gas-phase C_2H_4 species and a surfacebound C_2* species are formed upon $^2C-^2C$ cleavage

$$CH_2^*CH_2CH_2CH_x^* \rightarrow CH_2CH_2(g) + CH_2^*CH_x^*$$
$$(28)$$
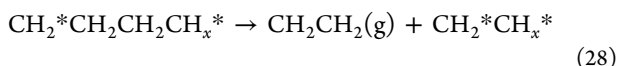
Long C−M distances in the transition state between the C−C bond being cleaved and the Ir surface lead to $\Delta H^{\ddagger}$ values (385, 352, and 337 kJ mol^{-1} for x values of 0, 1, and 2), which are much larger than for C−C cleavage via the α,β-bound $CH_3C^*C^*CH_3$ intermediate of butane (220 kJ mol^{-1}) in which both C atoms in the C−C bond are attached to the surface.

$^2C-^2C$ bonds may also activate in α,δ-bound intermediates in which both terminal ^1C atoms have lost more than one H atom, i.e., $CH_x^*CH_2CH_2CH_y^*$ species ($x = 0-1$, $y = 0-1$)

$$CH_x^*CH_2CH_2CH_y^* + * \rightarrow CH_2^*CH_x^* + CH_2^*CH_y^*$$
$$(29)$$
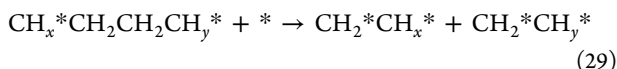
and such activations require four surface atoms to bind. The transition states for $^2C-^2C$ cleavage in $CH^*CH_2CH_2C^*$ and $C^*CH_2CH_2C^*$ give $\Delta H^{\ddagger}$ values (377 and 339 kJ mol^{-1}) much larger than that for C−C cleavage in α,β-bound $CH_3C^*C^*CH_3$ (220 kJ mol^{-1}). These α,δ-bound intermediates lose two to six H atoms (y) and require two to four binding sites (l), resulting in λ values ranging from 2 to 5. The corresponding $\Delta S^{\ddagger}$ values increase with increasing λ (from 24 to 279 J mol^{-1} K^{-1} as λ increased from 2 to 5), leading to a concomitant decrease in $\Delta G^{\ddagger}$ values (from 370 to 174 kJ mol^{-1}) for $^2C-^2C$ activations of α,δ-bound intermediates. The smallest $\Delta G^{\ddagger}$ (174 kJ mol^{-1}) for $^2C-^2C$ cleavage was observed for the α,δ-bound species, in which the terminal C atoms are completely dehydrogenated

($C^*CH_2CH_2C^*$ species) because this species releases the most $H_2(g)$ ($y = 6$, $l = 4$, $\lambda = 5$) and thus gives the greatest $\Delta S^{\ddagger}$. This $\Delta G^{\ddagger}$ value, however, is still larger than for $^2C-^2C$ activation in α,β-bound $CH_3C^*C^*CH_3$ (146 kJ mol^{-1}). Nine different $^1C-^2C$ cleavage reactions of α,δ-bound $CH_x^*CH_2CH_2CH_y^*$ ($x = 0-2$, $y = 0-2$) intermediates were also examined. These reactions also show much larger $\Delta H^{\ddagger}$ (318−422 kJ mol^{-1}) and $\Delta G^{\ddagger}$ (258−390 kJ mol^{-1}) values than for $^1C-^2C$ cleavage in α,β-bound $CH_3CH_2C^*CH^*$ species ($\Delta H^{\ddagger}$ and $\Delta G^{\ddagger}$ of 215 and 146 kJ mol^{-1}, respectively). These results indicate that $^2C-^2C$ cleavage in α,δ-bound intermediates does not contribute to measured *n*-butane hydrogenolysis rates.

3.3.2. C−C Bond Cleavage in n-Butane. $C_4H_x^*$ ($x = 0-10$) intermediates can cleave C−C bonds via 225 distinct elementary steps, which include more than 100 steps involving α,β,δ-bound (Figure 1g) and $\alpha,\beta,\gamma,\delta$-bound (Figure 1h) intermediates. Such diverse routes pose computational hurdles that render a comprehensive examination of all transition state structures impractical and, as we propose below, unnecessary. Many of these routes can actually be ruled out from their reaction free energies to form C_1, C_2, and C_3 fragments because their activation free energies must exceed such values; a similar approach was used to eliminate 2,3-dimethylbutane hydrogenolysis pathways in previous work.[26] The cleavage of $^1C-^2C$ bonds in *n*-butane forms C_1 and C_3 intermediates on the Ir surface

$$C_4H_{10} + lH^* \rightarrow C_3H_x^{la}* + CH_y^{lb}* + \lambda H_2$$
$$(30)$$
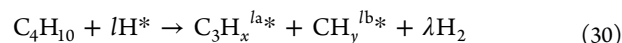
while $^2C-^2C$ cleavage forms C_2 species
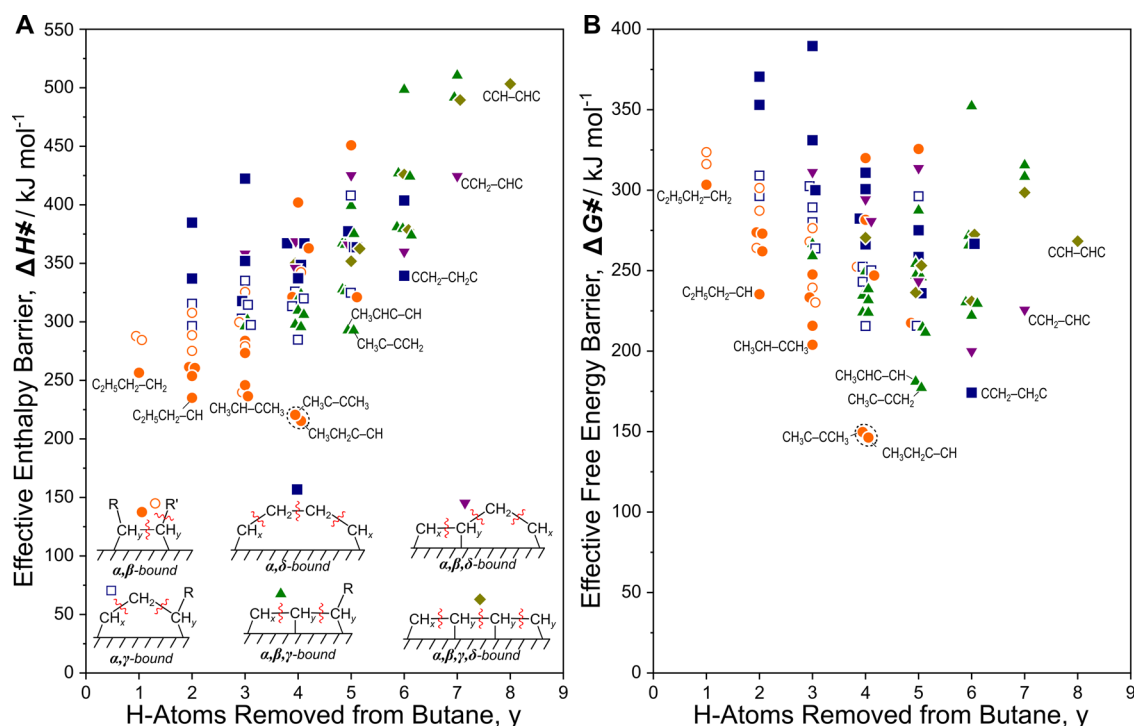
Figure 6. (a) $\Delta H^{\ddagger}$ and (b) $\Delta G^{\ddagger}$ values for C−C cleavage in butane-derived intermediates via: α,β-bound intermediates (●, orange for activations at α,β positions, ○ for activations at β,γ positions, i.e., between a bound C atom and an unbound C atom); α,γ-bound intermediates (□, blue); α,δ-bound intermediates (■, blue); α,β,γ-bound intermediates (▲, green); α,β,δ-bound intermediates (▼, purple); and $\alpha,\beta,\gamma,\delta$-bound intermediates (◆, brown). Notable transition states are labeled.

$$C_4H_{10} + lH^* \rightarrow C_2H_x^{\,la}* + C_2H_y^{\,lb}* + \lambda H_2 \qquad (31)$$
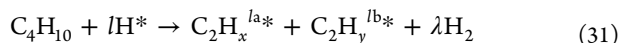
All structures of alkane-derived C_1–C_3 intermediates have been isolated in examinations of ethane[22] and propane hydrogenolysis (Section 3.2.3). The C−C cleavage transition state energies must be higher than the product states in eqs 30 and 31 because reverse barriers are ≥0 kJ mol^{-1}. Thus, we first calculate the reaction enthalpies and free energies to form all possible C_1–C_3 products of C−C cleavage and the corresponding stoichiometric λ number of $H_2(g)$ molecules from gaseous n-butane (ΔH_P and ΔG_P)

$$\Delta H_P = H[C_3H_x^{\,la}*] + H[CH_y^{\,lb}*] + \lambda H[H_2] - H[C_4H_{10}] \\ - lH[H*] \qquad (32)$$

$$\Delta H_P = H[C_2H_x^{\,la}*] + H[C_2H_y^{\,lb}*] + \lambda H[H_2] \\ - H[C_4H_{10}] - lH[H*] \qquad (33)$$

$$\Delta G_P = G[C_3H_x^{\,la}*] + G[CH_y^{\,lb}*] + \lambda G[H_2] - G[C_4H_{10}] \\ - lG[H*] \qquad (34)$$

$$\Delta G_P = G[C_2H_x^{\,la}*] + G[C_2H_y^{\,lb}*] + \lambda G[H_2] \\ - G[C_4H_{10}] - lG[H*] \qquad (35)$$

These ΔH_P and ΔG_P values represent lower bounds for the respective activation barriers ($\Delta H^{\ddagger}$ and $\Delta G^{\ddagger}$). ΔH_P increases systematically with the extent of dehydrogenation (Figure 5a) because of the endothermic nature of those H-removal steps; yet, ΔH_P values for cleavage via RC*−C*R′‡ (after removal of four H atoms) are smaller than for any other steps for both ^{1}C−^{2}C and ^{2}C−^{2}C cleavage. ΔG_P values (Figure 5b) reflect the

entropy benefits brought forth by $H_2(g)$ evolution are also smallest for C−C cleavage steps mediated by RC*−C*R′‡. The cleavage of ^{1}C−^{2}C and ^{2}C−^{2}C bonds via α,β-bound RC*−C*R′‡ transition states occurs with $\Delta G^{\ddagger}$ values of 144 and 148 kJ mol^{-1}, respectively. In what follows, we consider all C−C cleavage reactions of α,β,δ-bound (Figure 1g) and $\alpha,\beta,\gamma,\delta$-bound (Figure 1h) intermediates with ΔG_P below 145 kJ mol^{-1} because other steps would exhibit larger ΔG_P (and thus $\Delta G^{\ddagger}$) values larger than for routes mediated by α,β-bound RC*−C*R′‡ transition states. As a result, the discarded routes will not detectably contribute to hydrogenolysis rates.

In total, transition state energies (and ΔH_P and ΔG_P values) were determined for 18 C−C cleavage reactions of α,β,δ-bound intermediates (Figure 1g) and 16 C−C cleavage reactions of $\alpha,\beta,\gamma,\delta$-bound intermediates (Figure 1h). Their $\Delta H^{\ddagger}$ (317−503 kJ mol^{-1}) and $\Delta G^{\ddagger}$ (198−312 kJ mol^{-1}) (Tables S5 and S6) values are much higher than for routes involving C_2H_5C*−$CH*^{\ddagger}$ transition states (215 and 144 kJ mol^{-1}, respectively). The reactions with the lowest $\Delta G^{\ddagger}$ values among cleavages of α,β,δ-bound intermediates

$$CH_2*C*CH_2C* + * \rightarrow 2CH_2*C* \qquad (36)$$

and among cleavages of $\alpha,\beta,\gamma,\delta$-bound intermediates

$$CH*CH*CH*C* \rightarrow CH*CH*C* + CH* \qquad (37)$$

have λ values of 5.0 ($l = 4$, $y = 6$) and 5.5 ($l = 4$, $y = 7$), respectively, inconsistent with measured values (3.0 ± 0.2).[28] These data indicate that C−C cleavage in α,β,δ-bound and $\alpha,\beta,\gamma,\delta$-bound intermediates do not contribute to observed butane hydrogenolysis rates.

The transition states for 122 C−C activations of species derived from n-butane reactants were isolated (Figure 6). C−C rupture via RC*−C*R′‡ transition states gave the lowest $\Delta H^{\ddagger}$

barrier values (215 and 221 kJ mol^{-1} for ^{1}C–^{2}C cleavage) (Figure 6a) and $\Delta G^{\ddagger}$ barriers (139 and 146 kJ mol^{-1} for ^{1}C–^{2}C and ^{2}C–^{2}C cleavage) (Figure 6b) among all routes considered. The next most productive route (^{2}C–^{2}C activation in α,δ-bound *CCH$_2$CH$_2$C*) showed larger $\Delta G^{\ddagger}$ barriers (by 28 kJ mol^{-1}) than for steps mediated by RC*–C*R′ transition states; thus, we conclude that n-butane hydrogenolysis occurs predominately via RC*–C*R′ transition states, as in the case of ethane (R = R′ = H)[22] and propane (R = CH$_3$, R′ = H) (Figure 4c) reactants.

3.4. Effects of Chain Length on n-Alkane Hydrogenolysis Rates.

These findings, taken together with previous rate data and theoretical studies,[19,22,28] indicate that C–C cleavage in ethane, propane, and n-butane (and plausibly larger n-alkanes) preferentially involves α,β-bound RC*C*R′ species. In spite of these similar intermediates, n-alkane hydrogenolysis turnover rates increase with chain length, concurrently with a decrease in $\Delta H^{\ddagger}$ (257–214 kJ mol^{-1} from C$_2$ to C$_{10}$) and an increase in $\Delta S^{\ddagger}$ (171–259 J mol^{-1} K^{-1} from C$_2$ to C$_{10}$) with increasing chain length,[28] leading to $\Delta G^{\ddagger}$ values (156 kJ mol^{-1} for C$_2$ and 60 kJ mol^{-1} for C$_{10}$) and higher turnover rates for larger chains. The lower $\Delta H^{\ddagger}$ values were previously attributed to the different bond dissociation energies (BDEs) of the C–C bonds being cleaved[28] because more rigorous assessments were unavailable. Next, we examine the basis for these effects of chain length (and of C atom substitution) on $\Delta H^{\ddagger}$, $\Delta S^{\ddagger}$, and $\Delta G^{\ddagger}$ values for n-alkanes.

Ethane-derived CH*CH* species bind onto three surface atoms in an (η^2,η^2) configuration on Ir(111) surfaces; binding energies are similar at hcp (−194 kJ mol^{-1}) or fcc (−193 kJ mol^{-1}) 3-fold sites (hcp sites contain an atom in the second surface layer beneath the complex). The formation of CH*CH* (and three H$_2$ molecules) from ethane on H*-covered surfaces

$$CH_3CH_3 + 2H^* \rightleftharpoons CH^*CH^* + 3H_2 \qquad (38)$$

occurs with a ΔH_{rxn} of 156 kJ mol^{-1} (Figure 5a) and a ΔS_{rxn} of 126 J mol^{-1} K^{-1} (ΔG_{rxn} = 81 kJ mol^{-1}). These CH*CH* species shift from an (η^2,η^2) to an (η^3,η^3) binding mode as the CH*–CH*‡ transition state forms (Figure 7A); both C atoms in this transition state bind to three Ir atoms, and the C–C bond cleaves with a $\Delta H^{\ddagger}$ of 218 kJ mol^{-1} to give two CH* fragments (bound at adjacent fcc and hcp sites). Structures for RC*C*R′ intermediates derived from propane and butane (Figure 7B–D) resemble those derived from ethane in the C–M distance and binding mode; these structures, together with their energies, are shown in Figure 7. The geometry of the transition states formed from RC*C*R′ species have similar C–C and C–M bond lengths as those that mediate ^{2}C–^{2}C cleavage in cyclohexane (Ir(111); Figure 7E) and ^{2}C–^{2}C cleavage in methylcyclopentane (Pt(111)[30−32]).

DFT-derived $\Delta H^{\ddagger}$ values for C–C activation in C$_2$–C$_8$ n-alkanes via RC–CR′‡ complexes depend weakly on chain length, and their magnitudes do not change systematically with chain length, in contrast with measured values (from 257 to 221 kJ mol^{-1} for C$_2$ to C$_8$; Table 1, 0.7 nm Ir clusters[28]). The trends measured $\Delta H^{\ddagger}$ values which are consistent with the systematic weakening of C–C bonds in larger alkanes (i.e., BDE(C$_2$H$_6$) = 378 kJ mol^{-1}, BDE(C$_4$H$_{10}$) = 343 kJ mol^{-1} for the central C–C bond). BDE values, however, reflect the stability of the free radicals formed and thus neglect interactions between these fragments and surfaces in their adsorbed analogues. Thermochemical cycles (Figure 8) are used to

	Reactants	Transition State	Products
A			
ΔH (kJ mol^{-1})	156	218	122
ΔS (J mol^{-1} K^{-1})	126	136	126
ΔG (kJ mol^{-1})	81	137	48
B			
ΔH (kJ mol^{-1})	142	207	99
ΔS (J mol^{-1} K^{-1})	124	125	121
ΔG (kJ mol^{-1})	69	139	27
C			
ΔH (kJ mol^{-1})	145	210	103
ΔS (J mol^{-1} K^{-1})	119	111	119
ΔG (kJ mol^{-1})	74	144	33
D			
ΔH (kJ mol^{-1})	138	215	87
ΔS (J mol^{-1} K^{-1})	128	113	138
ΔG (kJ mol^{-1})	62	148	5
E			
ΔH (kJ mol^{-1})	132	207	94
ΔS (J mol^{-1} K^{-1})	129	118	121
ΔG (kJ mol^{-1})	56	137	22
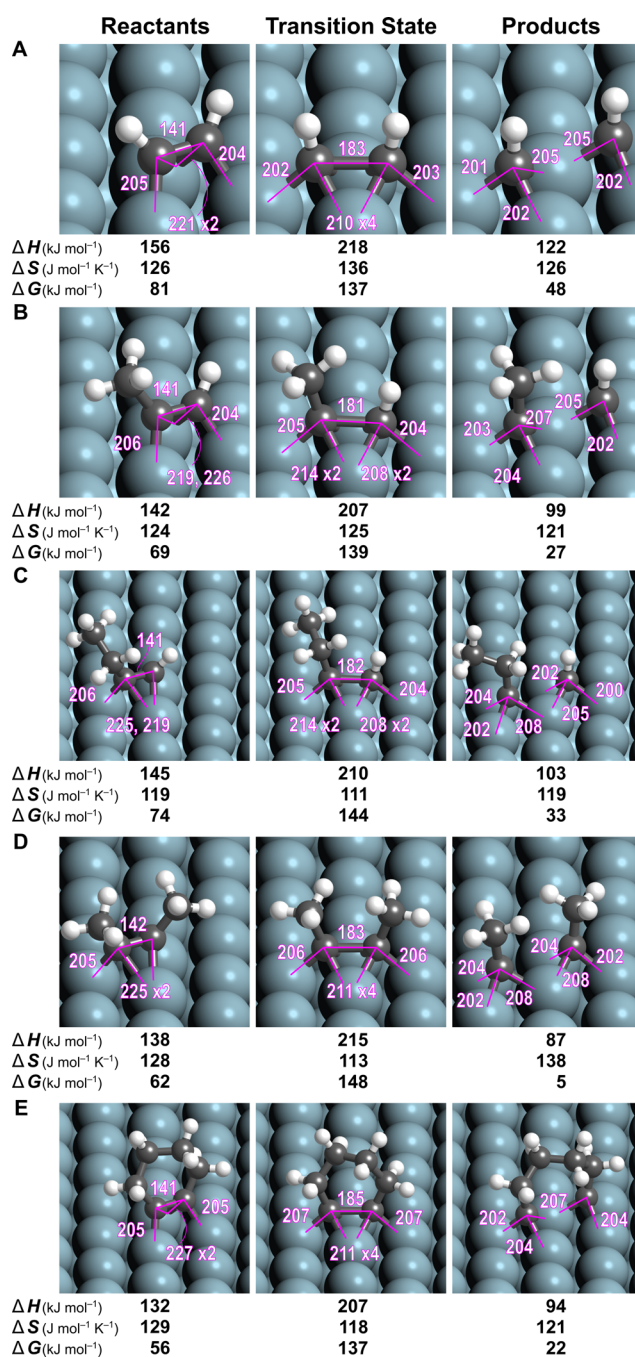
Figure 7. Reactant, transition, and product state structures for C–C activation in RCCR′ intermediates derived from (A) ethane, (B) propane, (C and D) butane, and (E) cyclohexane. Shown beneath each image are the ΔH (kJ mol^{-1}), ΔS (J mol^{-1} K^{-1}), and ΔG (kJ mol^{-1}) values for the formation of each species (and three H$_2$(g) molecules) from the alkane reactant and a H*-covered surface.

dissect $\Delta H^{\ddagger}$ values into those for convenient hypothetical steps that rigorously describe the activation enthalpies (and free energies) because of the state function nature of these thermodynamic properties. These $\Delta H^{\ddagger}$ values are given by the sum of the enthalpies for (i) desorption of two H* atoms as H$_2$(g) ($-\Delta H_{\text{ads,H2}}$); (ii) dehydrogenation of the gaseous n-alkane to molecule with the number and location of the missing H atoms at the transition state (an alkyne when four H atoms are removed (ΔH_{deh})); (iii) adsorption of this alkyne (ΔH_{ads})

Table 1. Enthalpies ($\Delta H^\ddagger$), Entropies ($\Delta S^\ddagger$), and Free Energies ($\Delta G^\ddagger$) Required to Form C—C Cleavage Transition States from Gas-Phase Alkanes and a H*-Covered Surface

	predicted			measured[c,19,22,28]		
	$\Delta H^{\ddagger a}$	$\Delta S^{\ddagger b}$	$\Delta G^{\ddagger b}$	$\Delta H^\ddagger$	$\Delta S^\ddagger$	$\Delta G^\ddagger$
reaction	kJ mol^{-1}	J mol^{-1} K^{-1}	kJ mol^{-1}	kJ mol^{-1}	J mol^{-1} K^{-1}	kJ mol^{-1}
CH*CH* → 2CH*	218	136	137	213 ± 2^d	141 ± 5^d	130 ± 5^d
				257 ± 3	171 ± 5	156 ± 6
CH$_3$C*CH* → CH$_3$C* + CH*	207	125	139	230 ± 3	164 ± 5	133 ± 6
C$_2$H$_5$C*CH* → C$_2$H$_5$C* + CH*	210	111	144	228 ± 3	181 ± 5	120 ± 6
CH$_3$C*C*CH$_3$ → 2CH$_3$C*	215	113	148	230 ± 3	195 ± 5	114 ± 6
C$_2$H$_5$C*C*CH$_3$ → C$_2$H$_5$C* + CH$_3$C*	220	103	159	–	–	–
C$_2$H$_5$C*C*C$_2$H$_5$ → 2 C$_2$H$_5$C*	226	100	166	213 ± 3	182 ± 5	105 ± 6
C$_3$H$_7$C*C*C$_2$H$_5$ → C$_3$H$_7$C* + C$_2$H$_5$C*	225	105	163	–	–	–
C$_3$H$_7$C*C*C$_3$H$_7$ → 2C$_3$H$_7$C*	219	104	157	221 ± 3	249 ± 5	73 ± 6
--C$_2$H$_4$C*C*C$_2$H$_4$-- → C*C$_4$H$_8$C*^{e}	207	118	137	–	–	–

^{a}Calculated at 593 K. ^{b}593 K, 1 bar H$_2$ and alkane. ^{c}On 0.7 nm Ir. ^{d}On 7 nm Ir. ^{e}Cyclohexane activation. -- indicates a bond.
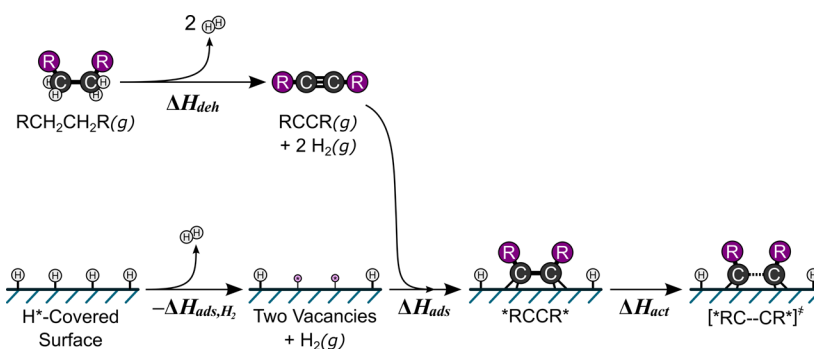
Figure 8. Born—Haber cycle for the formation of the RC—CR′ activation transition state.

Table 2. DFT-Derived Dehydrogenation Enthalpies to Form an Alkyne (ΔH_{deh}), Its Adsorption Enthalpy (ΔH_{ads}), the Intrinsic Activation Enthalpy (ΔH_{act}), and the Overall Activation Enthalpy for C—C Activation ($\Delta H^\ddagger$) of Ethane, Propane, and Butane^a

		ΔH_{deh}	ΔH_{ads}	$\Delta H_{ads+deh}$	ΔH_{act}	$\Delta H^{\ddagger b}$
reaction	C—C	kJ mol^{-1}	kJ mol^{-1}	kJ mol^{-1}	kJ mol^{-1}	kJ mol^{-1}
CH*CH* → 2CH*	^{1}C—^{1}C	316	−194	122	62	218
CH$_3$C*CH* → CH$_3$C* + CH*	^{2}C—^{1}C	280	−170	110	67	211
C$_2$H$_5$C*CH* → C$_2$H$_5$C* + CH*	^{2}C—^{1}C	282	−171	111	70	215
CH$_3$C*C*CH$_3$ → 2CH$_3$C*	^{2}C—^{2}C	247	−143	104	83	221

^{a}Enthalpies Determined at 593 K. $^b\Delta H^\ddagger$ related to other enthalpies by eq 39 with $-\Delta H_{ads,H2} = 34$ kJ mol^{-1}.

in an (η^2, η^2) binding mode; and (iv) the formation of the transition state from the adsorbed alkyne intermediate (ΔH_{act})

$$\Delta H^\ddagger = -\Delta H_{ads,H2} + \Delta H_{deh} + \Delta H_{ads} + \Delta H_{act} \quad (39)$$

Table 2 shows that longer chains give lower ΔH_{deh} values that are smaller for 2-butyne (247 kJ mol^{-1}) than 1-butyne (283 kJ mol^{-1}), the latter resembling that for propyne formation from propane (280 kJ mol^{-1}). Therefore, ΔH_{deh} values reflect the nature of the substituents at each C atom involved in the triple bond (Table 2). ΔH_{ads} becomes less negative with increasing C atom substitution, apparently due to steric effects (Table 2). The effects of chain length on ΔH_{deh} and ΔH_{ads} tend to compensate and lead to a slight decrease in their sum from C$_2$ to C$_4$ alkanes (Table 2). The activation barriers to form the C—C cleavage transition states from adsorbed alkyne precursors (ΔH_{act}) increase slightly with increasing chain length and offset the small decrease in (ΔH_{ads} + ΔH_{deh}). The collective contributions of these three terms (eq 39) do not lead to

systematic changes in $\Delta H^\ddagger$ with chain length. We conclude that BDE differences among C—C bonds do not lead to changes in C—C bond cleavage rates on Ir(111) surfaces; the measured effects of chain length on $\Delta H^\ddagger$ thus require a different explanation.

The RPBE functional used neglects attractive dispersive forces known to vary with chain length[67] because of van der Waals interactions between alkyl chains and surfaces. Their magnitudes are similar for adsorbed species of similar size;[67] therefore, they do not influence relative $\Delta H^\ddagger$ (and $\Delta G^\ddagger$) values among competing routes for a given alkane and do not affect the conclusions about the preferred route for each n-alkane. Dispersive forces, however, would decrease $\Delta H^\ddagger$ values more strongly with increasing alkane chain length. Indeed, such forces increase n-alkane heats of adsorption by 10−15 kJ mol^{-1} per C atom, as measured on Pt(111)[68] and obtained by theory on (111) surfaces of Cu, Au, and Pt.[67] These effects would offset any repulsive interactions due to steric effects (Table 1),

Table 3. Enthalpies[a] (kJ mol^{-1}) Required to Desorb H* and Form C−C Cleavage Transition States from Gas-Phase Alkanes and a H*-Covered Surface ($\Delta H^{\ddagger}$)

reaction	measured[b19,22,28]	RPBE	optB88-vdW	optB86b-vdW	vdW-DF2	BEEF
2H* → 2* + H$_2$(g)		34	57	69	14	109
CH*CH* → 2CH* ($\Delta H^{\ddagger}$)	213 ± 2[c]	218	183	168	229	317
	257 ± 3					
C$_2$H$_5$C*C*C$_2$H$_5$ → 2C$_2$H$_5$C* ($\Delta H^{\ddagger}$)	213 ± 3	226	115	98	175	268
difference (C$_2$−C$_6$)	44 ± 3[b]	−8	68	70	54	49

[a]Calculated at 593 K. [b]On 0.7 nm Ir. [c]On 7 nm Ir.

thus leading to smaller $\Delta H^{\ddagger}$ (and $\Delta G^{\ddagger}$) than reported above and preferentially so for the larger alkanes.

These dispersive interactions can be incorporated into DFT methods as semiempirical correction (e.g., DFT-D3[69,70]) or by using functionals that include van der Waals terms such as, e.g., optB88-vdW.[50] Here, we estimate $\Delta H^{\ddagger}$ values for *n*-hexane and ethane using optB88-vdW,[50] optB86b-vdW,[51] vdW-DF2,[52] and BEEF[53] functionals (Table 3). $\Delta H^{\ddagger}$ values using the RPBE functional differ by −8 kJ mol^{-1} between ethane and hexane ($\Delta H^{\ddagger}_{C2} - \Delta H^{\ddagger}_{C6}$), in contrast with measurements (+44 kJ mol^{-1} on 0.7 nm Ir;[19,22,28] Table 1). The average ($\Delta H^{\ddagger}_{C2} - \Delta H^{\ddagger}_{C6}$) value using all functionals that account for dispersive forces is +60 kJ mol^{-1} (Table 3). This value is slightly larger than measured differences (+44 ± 3 kJ mol^{-1}) but much closer to experimental values than with RPBE functionals (−8 kJ mol^{-1}). Calculated $\Delta H^{\ddagger}$ values for ethane hydrogenolysis range from 168 to 316 kJ mol^{-1}, with no methods coming closer to measured values (213 kJ mol^{-1}; 7 nm Ir[19]) than the RPBE functional. $\Delta H^{\ddagger}$ values depend on H* desorption enthalpy ($-\Delta H_{ads,H2}$)

$$\Delta H^{\ddagger} = H[\text{TS}^{*\ddagger}] + 3H[\text{H}_2(\text{g})] - \Delta H_{ads,H2}$$
$$- H[\text{Alkane}(\text{g})] \tag{40}$$

and the large range in calculated $-\Delta H_{ads,H2}$ values (14−109 kJ mol^{-1}) partially results in the large range in $\Delta H^{\ddagger}$ values reported. Ultimately, the van der Waals functionals accurately predict changes in $\Delta H^{\ddagger}$ values with increasing chain length while sacrificing accuracy in absolute $\Delta H^{\ddagger}$ values. Of course, the remarkable agreement between measured $\Delta H^{\ddagger}$ values and those calculated by RPBE methods are likely the result of a cancellation of errors: The RPBE functional lacks attractive van der Waals interactions between the transition state and the metal surface, and our catalyst model lacks repulsive interactions between the transition state and coadsorbed H*. The calculated decreases in $\Delta H^{\ddagger}$ with increasing chain size for functionals which include dispersive interactions confirm that such dispersive interactions between alkyl chains and the metal surface are what lead to decreases in measured $\Delta H^{\ddagger}$ values rather than the decrease in C−C BDE values, as was previously implicated.[28]

Measured $\Delta H^{\ddagger}$ values decrease with increasing chain length, but $\Delta S^{\ddagger}$ values increase monotonically (171−259 J mol^{-1} K^{-1} for C$_2$ to C$_{10}$ *n*-alkanes, Table 1). These $\Delta S^{\ddagger}$ values depend on the entropies of gaseous alkanes and H$_2$ and on the entropies of chemisorbed H* and RC*−C*R′‡ transition states

$$\Delta S^{\ddagger} = S[\text{RC}^*-\text{C}^*\text{R}'^{\ddagger}] + \lambda S[\text{H}_2(\text{g})] - 2S[\text{H}^*]$$
$$- S[\text{C}_n\text{H}_{2n+2}(\text{g})] \tag{41}$$

DFT-derived vibrational frequencies are used to estimate the entropies of adsorbed RC*−C*R′‡ transition states (for C$_2$−

C$_8$ *n*-alkanes and cyclohexane). Statistical mechanics formalisms are used for entropies for gaseous alkanes and H$_2$. The entropy of H* at high coverages was estimated (as 55 J mol^{-1} K^{-1} per H* on Ir(111)) by direct integration of potential energy surfaces.[20] These $\Delta S^{\ddagger}$ estimates (Table 1) decrease gradually with increasing chain length (136−104 J mol^{-1} K^{-1} from C$_2$ to C$_8$).[27] Measured $\Delta S^{\ddagger}$ values depend sensitively on Ir cluster size (30 J mol^{-1} K^{-1} smaller on 7 nm than on 0.7 nm Ir clusters; Table 1)[20,27] and, in contrast with theoretical estimates, actually increase with chain length (171 to 249 J mol^{-1} K^{-1} from C$_2$ to C$_8$). Theoretical $\Delta S^{\ddagger}$ estimates for ethane hydrogenolysis on Ir(111) (136 J mol^{-1} K^{-1}) agree well with those measured on large Ir clusters (141 J mol^{-1} K^{-1}), consistent with the prevalence of low-index planes on large metal particles. The measured effects of chain length on $\Delta S^{\ddagger}$, however, are not described well by the DFT and statistical mechanics methods used here, even though measured and theoretical λ values and the H$_2$ desorption events that account for these λ values significantly contribute to $\Delta S^{\ddagger}$. We surmise that these discrepancies reflect the inaccurate predictions of the frequencies of weak modes consisting of hindered translations and rotations by periodic DFT methods; such modes significantly contribute to the entropy of the RC*−C*R′‡ transition states. The difference in $\Delta S^{\ddagger}$ between ^{1}C−^{2}C and ^{2}C−^{2}C cleavage of butane is predicted to be −2 J mol^{-1} K^{-1}, whereas that measured is +14 J mol^{-1} K^{-1}, indicating that DFT inaccuracies in entropy estimates persist even for the relatively small −CH$_3$ rotors present in such structures; as a result, DFT indicates a preference for ^{1}C−^{2}C activation, even though measurements show higher rates for ^{2}C−^{2}C cleavage. Purely statistical mechanics treatments using rigid-rotor approximations within RC*−C*R′‡ transition states led to excellent agreement between measured values and theoretical estimates of $\Delta S^{\ddagger}$.[28]

The systematic isolation of more than 150 C−C cleavage transition states in *n*-alkanes and cycloalkanes demonstrates that ^{1}C−^{1}C, ^{1}C−^{2}C, and ^{2}C−^{2}C bonds cleave via RC*−C*R′‡ transition states of similar structure and extent of dehydrogenation. The effects of chain length on reactivity do not reflect concomitant changes in C−C bond dissociation energies in reactants but reflect instead the stabilization of transition states via dispersive forces that strengthen with alkane size, thus requiring theoretical treatments that accurately capture van der Waals interactions. Finally, the measured effects of $\Delta S^{\ddagger}$ values reflect both the number of H$_2$ molecules formed with transition states (H$_2$) and transition state entropy uncaptured by purely vibrational frequency treatments of such transition states.

■ CONCLUSIONS

Enthalpies ($\Delta H^{\ddagger}$) and free energies ($\Delta G^{\ddagger}$) to form C−C cleavage transition states within >150 propane- and butane-derived intermediates demonstrate that ^{1}C−^{2}C and ^{2}C−^{2}C

bonds in alkanes proceed via C−C cleavage of α,β-bound (η^2, η^2) RC*C*R' intermediates. These results are consistent with previous findings for $^1C-^1C$ activations for ethane, indicating that C_2-C_4 n-alkanes activate via homologous mechanisms. The RC*−C*R'‡ transition states that mediate C−C cleavage in n-alkanes require two sites on the catalyst surface and have four fewer H atoms than their alkane reagents, resulting in three H_2 molecules formed with each transition state formation when metal surfaces are saturated in H*. This formation of H_2 leads to rates inhibited by $(H_2)^3$, and such a dependence is observed for $^1C-^1C$, $^1C-^2C$, and $^2C-^2C$ bond cleavage within C_2-C_{10} n-alkanes, branched alkanes, and cycloalkanes.[19] Measured decreases in $\Delta H^{\ddagger}$ with increasing alkane chain length reflect stabilizing dispersive interactions between the alkyl chains present in RC*−C*R'‡ transition states and the catalyst surface rather than any intrinsic weakening (such as those measured by bond dissociation energies) of the C−C bonds. Previous work has also demonstrated that long alkyl chains (such as those present during activations of longer n-alkanes) contribute significantly to the entropy of the adsorbed transition states, leading to increasing $\Delta S^{\ddagger}$ values with increasing n-alkane chain size.[28] These effects are not captured by traditional vibrational frequency calculations used to determine entropies of adsorbed states, demonstrating the need to improve those approaches.

Bonds of branched species (such as isobutane or 2,3-dimethylbutane) containing ^3C atoms cannot form these α,β-bound (η^2, η^2) RC*C*R' intermediates. These species must then sacrifice additional H atoms in the form of C−H activations at C-positions away from the bond being broken, resulting in an increase in entropy, which decreases free energies for transition state formation and leads to greater inhibition by H_2 (rates proportional to $(H_2)^{-4}$ for isobutane and $(H_2)^{-4.3\pm0.3}$ for isobutane and 2,3-dimethylbutane hydrogenolysis).[19,26]

ASSOCIATED CONTENT

Ⓢ Supporting Information

The Supporting Information is available free of charge on the ACS Publications website at DOI: 10.1021/acs.jpcc.6b00323.

Effects of chain length on the mechanism and rates of metal-catalyzed hydrogenolysis of n-alkanes (PDF)

AUTHOR INFORMATION

Corresponding Author
*E-mail: iglesia@berkeley.edu.

Present Address
§Department of Chemical Engineering, University of Florida, Gainesville, FL 32611, United States.

Notes
The authors declare no competing financial interest.

ACKNOWLEDGMENTS

REFERENCES

(1) Weitkamp, J.; Jacobs, P. A.; Martens, J. A. Isomerization and hydrocracking of C_9 through C_{16} n-alkanes on platinum/HZSM-5 zeolite. *Appl. Catal.* **1983**, *8*, 123−141.

(2) McVicker, G. B.; Daage, M.; Touvelle, M. S.; Hudson, C. W.; Klein, D. P.; Baird, W. C.; Cook, B. R.; Chen, J. G.; Hantzer, S.; Vaughan, D. E. W.; Ellis, E. S.; Feeley, O. C. Selective ring opening of naphthenic molecules. *J. Catal.* **2002**, *210*, 137−148.

(3) Do, P. T.; Alvarez, W. E.; Resasco, D. E. Ring opening of 1,2- and 1,3-dimethylcyclohexane on iridium catalysts. *J. Catal.* **2006**, *238*, 477−488.

(4) Shi, H.; Gutierrez, O. Y.; Haller, G. L.; Mei, D.; Rousseau, R.; Lercher, J. A. Structure sensitivity of hydrogenolytic cleavage of endocyclic and exocyclic C-C bonds in methylcyclohexane over supported iridium particles. *J. Catal.* **2013**, *297*, 70−78.

(5) Shi, H.; Li, X.; Haller, G. L.; Gutierrez, O. Y.; Lercher, J. A. Active sites and reactive intermediates in the hydrogenolytic cleavage of C-C bonds in cyclohexane over supported iridium. *J. Catal.* **2012**, *295*, 133−145.

(6) Weisang, F.; Gault, F. G. Selective isomerization of methyl-pentanes on iridium catalysts. *J. Chem. Soc., Chem. Commun.* **1979**, 519−520.

(7) Speight, J. G. In *Kirck-Othmer Encyclopedia of Chemical Technology*; Kirk, R. E., Othmer, D. F., Eds.; John Wiley and Sons, Inc: New York, 2012; p 1−49.

(8) Iglesia, E.; Reyes, S. C.; Madon, R. J.; Soled, S. L. Selectivity control and catalyst design in the Fischer−Tropsch synthesis: sites, pellets, and reactors. *Adv. Catal.* **1993**, *39*, 221−302.

(9) Bond, G. C. *Metal-Catalysed Reactions of Hydrocarbons*; Springer: New York, 2005.

(10) Gault, F. G. Mechanisms of skeletal isomerization of hydrocarbons on metals. *Adv. Catal.* **1981**, *30*, 1−95.

(11) Cimino, A.; Boudart, M.; Taylor, H. Ethane hydrogenation-cracking on iron catalysts with and without alkali. *J. Phys. Chem.* **1954**, *58*, 796−800.

(12) Kemball, C.; Taylor, H. S. The catalytic decomposition of ethane and ethane-hydrogen mixtures. *J. Am. Chem. Soc.* **1948**, *70*, 345−351.

(13) Morikawa, K.; Benedict, W. S.; Taylor, H. S. Activation of specific bonds in complex molecules at catalytic surfaces. II. Carbon-hydrogen and carbon-carbon bonds in ethane and ethane-d. *J. Am. Chem. Soc.* **1936**, *58*, 1795−1800.

(14) Sinfelt, J. H. Specificity in catalytic hydrogenolysis by metals. *Adv. Catal.* **1973**, *23*, 91−119.

(15) Gault, F. G. Effect de la Dispersion du Platine sur le Support dans L'Hydrogenolyse des Hydrocarbures Cyclopentaniques. *C. R. Acad. Sci.* **1957**, *245*, 1620−1623.

(16) Maire, G.; Plouidy, G.; Prudhomme, J. C.; Gault, F. G. The mechanisms of hydrogenolysis and isomerization of hydrocarbons on metals. I. Hydrogenolysis of cyclic hydrocarbons. *J. Catal.* **1965**, *4*, 556−569.

(17) Kua, J.; Faglioni, F.; Goddard, W. A. Thermochemistry for Hydrocarbon Intermediates Chemisorbed on Metal Surfaces: $CH_{n-m}(CH_3)_m$ with $n = 1, 2, 3$ and $m \leq n$ on Pt, Ir, Os, Pd, Rh, and Ru. *J. Am. Chem. Soc.* **2000**, *122*, 2309−2321.

(18) Chorkendorff, I.; Niemantsverdriet, J. W. *Concepts of Modern Catalysis and Kinetics*, 2nd ed.; Wiley-VCH: New York, 2007.

(19) Flaherty, D. W.; Hibbitts, D. D.; Iglesia, E. Metal-catalyzed C-C bond cleavage in alkanes: effects of methyl substitution on transition-state structures and stability. *J. Am. Chem. Soc.* **2014**, *136*, 9664−9676.

(20) Foger, K.; Anderson, J. R. Hydrocarbon reactions on supported iridium catalysts. *J. Catal.* **1979**, *59*, 325−339.

(21) Sinfelt, J. H.; Taylor, W. F.; Yates, D. J. C. Catalysis over supported metals. III. Comparison of metals of known surface area for ethane hydrogenolysis. *J. Phys. Chem.* **1965**, *69*, 95−101.

(22) Flaherty, D. W.; Hibbitts, D. D.; Gürbüz, E. I.; Iglesia, E. Theoretical and kinetic assessment of the mechanism of ethane hydrogenolysis on metal surfaces saturated with chemisorbed hydrogen. *J. Catal.* **2014**, *311*, 350−356.

(23) Cortright, R. D.; Watwe, R. M.; Spiewak, B. E.; Dumesic, J. A. Kinetics of ethane hydrogenolysis over supported platinum catalysts. *Catal. Today* **1999**, *53*, 395−406.

(24) Cortright, R. D.; Watwe, R. M.; Dumesic, J. A. Ethane hydrogenolysis over platinum selection and estimation of kinetic parameters. *J. Mol. Catal. A: Chem.* **2000**, *163*, 91−103.

(25) Engstrom, J. R.; Goodman, D. W.; Weinberg, W. H. Hydrogenolysis of ethane, propane, n-butane, and neopentane on the (111) and (110)-(1 × 2) surfaces of iridium. *J. Am. Chem. Soc.* **1988**, *110*, 8305−8319.

(26) Hibbitts, D. D.; Flaherty, D. W.; Iglesia, E. Role of branching on the rate and mechanism of C−C cleavage in alkanes on metal surfaces. *ACS Catal.* **2016**, *6*, 469−482.

(27) Sinfelt, J. H. Kinetics of ethane hydrogenolysis. *J. Catal.* **1972**, *27*, 468−471.

(28) Flaherty, D. W.; Iglesia, E. Transition-state enthalpy and entropy effects on reactivity and selectivity in hydrogenolysis of n-alkanes. *J. Am. Chem. Soc.* **2013**, *135*, 18586−18599.

(29) Watwe, R. M.; Cortright, R. D.; Nørskov, J. K.; Dumesic, J. A. Theoretical studies of stability and reactivity of C_2 hydrocarbon species on Pt clusters, Pt(111), and Pt(211). *J. Phys. Chem. B* **2000**, *104*, 2299−2310.

(30) Zhao, Z.-J.; Moskaleva, L. V.; Rösch, N. Tuning the selectivity for ring-opening reactions of methylcyclopentane over Pt catalysts: A mechanistic study from first-principles calculations. *J. Catal.* **2012**, *285*, 124−133.

(31) Zhao, Z.-J.; Moskaleva, L. V.; Rösch, N. Formation of n-hexane from methylcyclopentane via a metallacyclobutane intermediate at step sites of Pt surfaces: Mechanism from first-principles calculations. *J. Catal.* **2013**, *299*, 146−149.

(32) Zhao, Z.-J.; Moskaleva, L. V.; Rösch, N. Ring-Opening Reactions of Methylcyclopentane over Metal Catalysts, M = Pt, Rh, Ir, and Pd: A Mechanistic Study from First-Principles Calculations. *ACS Catal.* **2013**, *3*, 196−205.

(33) Chen, Y.; Vlachos, D. G. Hydrogenation of ethylene and dehydrogenation and hydrogenolysis of ethane on Pt (111) and Pt (211): a density functional theory study. *J. Phys. Chem. C* **2010**, *114*, 4973−4982.

(34) Sinfelt, J. H.; Yates, D. J. C. Catalytic hydrogenolysis of ethane over the noble metals of Group VIII. *J. Catal.* **1967**, *8*, 82−90.

(35) Bond, G. C.; Cunningham, R. H. Alkane transformations on supported platinum catalysts. *J. Catal.* **1997**, *166*, 172−185.

(36) Bond, G. C.; Slaa, J. C. Catalytic and structural properties of ruthenium bimetallic catalysts: hydrogenolysis of propane and n-butane on Ru/Al$_2$O$_3$ catalysts modified by a Group 14 element. *J. Mol. Catal. A: Chem.* **1996**, *106*, 135−149.

(37) Boudart, M.; Ptak, L. D. Reactions of neopentane on transition metals. *J. Catal.* **1970**, *16*, 90−96.

(38) Flaherty, D. W.; Iglesia, E. Catalytic ring opening of cycloalkanes on Ir clusters: alkyl substitution effects on the structure and stability of C−C bond cleavage transition states. *J. Phys. Chem. C* **2015**, *119*, 2597−2613.

(39) Kresse, G.; Furthmuller, J. Efficiency of ab-initio total energy calculations for metals and semiconductors using a plane-wave basis set. *Comput. Mater. Sci.* **1996**, *6*, 15−50.

(40) Kresse, G.; Furthmuller, J. Efficient iterative schemes for ab initio total-energy calculations using a plane-wave basis set. *Phys. Rev. B: Condens. Matter Mater. Phys.* **1996**, *54*, 11169−11186.

(41) Kresse, G.; Hafner. Ab initio molecular dynamics for liquid metals. *Phys. Rev. B: Condens. Matter Mater. Phys.* **1993**, *47*, 558−561.

(42) Kresse, G.; Hafner. Ab initio molecular-dynamics simulation of the liquid-metal−amorphous-semiconductor transition in germanium. *Phys. Rev. B: Condens. Matter Mater. Phys.* **1994**, *49*, 14251−14269.

(43) Monkhorst, H. J.; Pack, J. D. Special points for Brillouin-zone integrations. *Phys. Rev. B* **1976**, *13*, 5188−5192.

(44) Blochl, P. E. Projector augmented-wave method. *Phys. Rev. B: Condens. Matter Mater. Phys.* **1994**, *50*, 17953−17979.

(45) Kresse, G.; Joubert, D. From ultrasoft pseudopotentials to the projector augmented-wave method. *Phys. Rev. B: Condens. Matter Mater. Phys.* **1999**, *59*, 1758−1775.

(46) Hammer, B.; Hansen, L.; Norskov, J. K. Improved adsorption energetics within density-functional theory using revised Perdew-Burke-Ernzerhof functionals. *Phys. Rev. B: Condens. Matter Mater. Phys.* **1999**, *59*, 7413−7421.

(47) Perdew, J.; Burke, K.; Ernzerhof, M. Generalized gradient approximation made simple. *Phys. Rev. Lett.* **1996**, *77*, 3865−3868.

(48) Zhang, Y.; Yang, W. Comment on "Generalized gradient approximation made simple. *Phys. Rev. Lett.* **1998**, *80*, 890.

(49) Klimeš, J.; Bowler, D.; Michaelides, A. Chemical accuracy for the van der Waals density functional. *J. Phys.: Condens. Matter* **2010**, *22*, 022201.

(50) Klimeš, J.; Bowler, D.; Michaelides, A. Van der Waals density functionals applied to solids. *Phys. Rev. B: Condens. Matter Mater. Phys.* **2011**, *83*, 195131.

(51) Lee, K.; Murray, E.; Kong, L.; Lundqvist, B.; Langreth, D. A density functional for sparse matter. *Phys. Rev. B: Condens. Matter Mater. Phys.* **2010**, *83*, 081101.

(52) Wellendorff, J.; Lundgaard, K. T.; Møgelhøj, A.; Petzold, V.; Landis, D.; Nørskov, J. K.; Bligaard, T.; Jacobsen, K. W. Density functionals for surface science: Exchange-correlation model development with Bayesian error estimation. *Phys. Rev. B: Condens. Matter Mater. Phys.* **2012**, *85*, 235149.

(53) Henkelman, G.; Jonsson, H. A. Improved tangent estimate in the nudged elastic band method for finding minimum energy paths and saddle points. *J. Chem. Phys.* **2000**, *113*, 9978−9985.

(54) Jonsson, H. A.; Mills, G.; Jacobsen, K. W. Nudged Elastic Band Method for Finding Minimum Energy Paths of Transitions. In *Classical and Quantum Dynamics in Condensed Phase Simulations*; Berne, B. J., Ciccotti, G., Coker, D. F., Eds.; World Scientific: 1998; p 385.

(55) Henkelman, G.; Jonsson, H. A. A dimer method for finding saddle points on high dimensional potential surfaces using only first derivatives. *J. Chem. Phys.* **1999**, *111*, 7010−7022.

(56) Anslyn, E. V.; Dougherty, D. A. *Modern Physical Organic Chemistry*; University Science Books: Sausalito, CA, 2006.

(57) Yang, M.; Somorjai, G. A. Adsorption and reactions of C6 hydrocarbons at high pressures on Pt (111) single-crystal surfaces studied by sum frequency generation vibrational spectroscopy: mechanisms of isomerization and dehydrocyclization of n-hexane. *J. Am. Chem. Soc.* **2004**, *126*, 7698−7708.

(58) Weiss, M. J.; Hagedorn, C. J.; Mikesell, P. J.; Little, R. D.; Weinberg, W. H. Decomposition of cyclobutane on Ru (001): Identification of a surface metallacycle. *J. Am. Chem. Soc.* **1998**, *120*, 11812−11813.

(59) Dowie, R. S.; Whan, D. A.; Kemball, C. Hydrogenolysis of saturated hydrocarbons on evaporated platinum films. *J. Chem. Soc., Faraday Trans. 1* **1972**, *68*, 2150−2162.

(60) Kemball, C. The Structure and Stability of Hydrocarbon Intermediates on the Surface of Catalysts. *Catal. Rev.: Sci. Eng.* **1972**, *5*, 33−53.

(61) Kemball, C.; Brown, R. Evidence for the formation of an $\alpha\delta$-adsorbed hydrocarbon intermediate on a rhodium catalyst. *J. Chem. Soc., Chem. Commun.* **1987**, 771−773.

(62) Anderson, J. R.; D.D. Eley, H. P.; Paul, B. W. Metal catalyzed skeletal reactions of hydrocarbons. *Adv. Catal.* **1973**, *23*, 1−90.

(63) McDermott, J. X.; White, J. F.; Whitesides, G. M. Preparation and thermal decomposition of platinum (II) metallacycles. *J. Am. Chem. Soc.* **1973**, *95*, 4451−4452.

(64) McDermott, J. X.; White, J. F.; Whitesides, G. M. Thermal decomposition of bis (phosphine) platinum (II) metallacycles. *J. Am. Chem. Soc.* **1976**, *98*, 6521−6528.

(65) Young, G. B.; Whitesides, G. M. Oxidative addition and reductive elimination reactions involving platinum metallacycles. *J. Am. Chem. Soc.* **1978**, *100*, 5808−5815.

(66) Grubbs, R. H.; Miyashita, A. Carbon-carbon bond cleavage reactions in the decomposition of metallacycles. *J. Am. Chem. Soc.* **1978**, *100*, 7418−7420.

(67) Lee, K.; Morikawa, Y.; Langreth, D. C. Adsorption of n-butane on Cu (100), Cu (111), Au (111), and Pt (111): Van der Waals density-functional study. *Phys. Rev. B: Condens. Matter Mater. Phys.* **2010**, *82*, 155461.

(68) Tait, S. L.; Dohnálek, Z.; Campbell, C. T.; Kay, B. D. n-alkanes on Pt (111) and on C(0001)/ Pt (111): Chain length dependence of kinetic desorption parameters. *J. Chem. Phys.* **2006**, *125*, 234308.

(69) Grimme, S.; Antony, J.; Ehrlich, S.; Krieg, H. A consistent and accurate ab initio parametrization of density functional dispersion correction (DFT-D) for the 94 elements H-Pu. *J. Chem. Phys.* **2010**, *132*, 154104.

(70) Grimme, S.; Ehrlich, S.; Goerigk, L. Effect of the damping function in dispersion corrected density functional theory. *J. Comput. Chem.* **2011**, *32*, 1456.